

WGLE: Backdoor-free and Multi-bit Black-box Watermarking for Graph Neural Networks

Tingzhi Li
Xidian University
tingzhi.li@stu.xidian.edu.cn

Xuefeng Liu
Xidian University
liuxf@mail.xidian.edu.cn

Abstract—Graph Neural Networks (GNNs) are increasingly deployed in graph-related applications, making ownership verification critical to protect their intellectual property against model theft. Fingerprinting and black-box watermarking are two main methods. However, the former relies on determining model similarity, which is computationally expensive and prone to ownership collisions after model post-processing such as model pruning or fine-tuning. The latter embeds backdoors, exposing watermarked models to the risk of backdoor attacks. Moreover, both methods enable ownership verification but do not convey additional information. As a result, each distributed model requires a unique trigger graph, and all trigger graphs must be used to query the suspect model during verification. Multiple queries increase the financial cost and the risk of detection.

To address these challenges, this paper proposes WGLE, a novel black-box watermarking paradigm for GNNs that enables embedding the multi-bit string as the ownership information without using backdoors. WGLE builds on a key insight we term Layer-wise Distance Difference on an Edge (LDDE), which quantifies the difference between the feature distance and the prediction distance of two connected nodes. By predefining positive or negative LDDE values for multiple selected edges, WGLE embeds the watermark encoding the intended information without introducing incorrect mappings that compromise the primary task. WGLE is evaluated on six public datasets and six mainstream GNN architectures along with state-of-the-art methods. The results show that WGLE achieves 100% ownership verification accuracy, an average fidelity degradation of 0.85%, comparable robustness against potential attacks, and low embedding overhead.

I. INTRODUCTION

Graph Neural Networks (GNNs) are extensively applied in a range of domains such as finance [1], [2], medicine [3], and social network analysis [4], [5], due to their ability to capture relational structures in graph data. Developing high-performance models necessitates substantial computational resources and large-scale datasets, making them valuable intellectual property (IP) susceptible to copyright infringement, such as unauthorized use or illicit copy. Therefore, well-developed GNN models are important intellectual property, and their copyright must deserve protection.

Ownership verification is widely adopted to protect model copyrights [6], [7]. Its objective is to determine whether the suspect model is an unauthorized copy of the original model or an independently trained one. For practical deployment, ownership verification is typically conducted in the black-box setting, where access to the model’s internal parameters or architecture is unavailable, and verification relies solely on querying the model and analyzing its predictions. Ownership

verification has shown notable success in models processing Euclidean data such as images, text, and video [8], [9], [10]. However, directly applying these methods to GNNs is infeasible due to the non-Euclidean nature of graph data, characterized by the complex and irregular structure of graphs and the sensitivity of GNNs to localized perturbations.

Existing Solutions. Recent studies address these challenges and extend ownership verification to GNN copyright protection [11], [12], [13], [14]. One line of methods [13], [14], known as GNN fingerprinting, constructs fingerprints based on the model’s unique properties that differ from other models, such as layer-wise node embeddings [13] or overall model behaviors [14]. The suspect model is identified as an unauthorized copy if it shares a substantially similar fingerprint to the fingerprinted model. The key strengths of GNN fingerprinting are backdoor-free and robust against model extraction attacks, as the construction of fingerprints does not introduce an additional objective into the training process. However, fingerprints require significant computational overhead to be constructed and are prone to ownership collisions when models are post-processed, such as model pruning or fine-tuning [15], [14], [16]. Therefore, GNN fingerprinting methods are limited in scenarios where the owner has limited computational resources [17], or the model is potentially subject to substantial fine-tuning or high-ratio pruning [18].

Another line of methods [11], [12] adapts backdoor attacks as watermarks, named GNN black-box watermarking. These methods embed backdoor patterns into certain nodes and assign incorrect labels for them. The watermark functions as an additional input-output mapping, causing samples containing the backdoor patterns to be misclassified into the designated class rather than their true class. The suspect model is identified as an unauthorized copy if it classifies a majority of such backdoor samples into the designated class. Backdoor-based watermarking methods offer stronger robustness against model post-processing and incur low computational overhead during the embedding process. However, using backdoor attacks as watermarks poses a serious security threat [19] to the primary task. Once the backdoor is exposed, malicious users can exploit it to manipulate the behavior of the model and force the desired outputs [20], [21].

Furthermore, both GNN fingerprinting and GNN black-box watermarking methods are limited by their zero-bit capacity, which enables ownership verification but cannot encode any additional information [7]. As a result, such methods incur

high financial costs [17] and increase the risk of detection during the verification process [22]. In addition, the ownership information is susceptible to forgery [23].

Our proposal. Motivated by the above analysis, we propose WGLE, a novel GNN black-box watermarking paradigm that inherits the advantages of low overhead and strong robustness from previous GNN black-box watermarking methods. Furthermore, WGLE (i) is backdoor-free, eliminating the security threats associated with backdoor attacks, and (ii) supports multi-bit capacity, which makes ownership verification financially inexpensive and hard to detect. The multi-bit watermark is more difficult to forge than the zero-bit watermark.

WGLE builds on a key insight, referred to as *Layer-wise Distance Difference on an Edge (LDDE)*, which quantifies the difference between the feature distance and the prediction distance of two connected nodes. LDDE is a suitable watermark carrier as it can be calculated in all GNNs and modified in a specified direction with a minor impact on the model’s performance in the primary task (details in Section IV). The owner first constructs a trigger graph based on the original model. For each model distribution, the watermark is generated and then embedded by fine-tuning the original model to modify the LDDE values of selected edges in the trigger graph. WGLE is backdoor-free, as there is no incorrect mapping that forces specific samples to be classified into the designated class; all samples remain correctly classified into their true classes. To achieve multi-bit capacity, WGLE transforms the signs of the LDDE values of selected edges in the trigger graph into a multi-bit string, also known as the watermark. The LDDE value of each edge is determined by the local topology and the node features surrounding it, so each edge exhibits an individual LDDE value.

Evaluations. We evaluated WGLE and state-of-the-art GNN black-box watermarking (WGB [12]) and fingerprinting methods (RBOVG [14]) across six mainstream GNN architectures and six real-world datasets. The experimental results show that WGLE achieves 100% ownership verification accuracy, consistent with WGB and RBOVG. In terms of fidelity, WGLE has a minor degradation in the accuracy of the primary task, with an average drop of 0.85% in accuracy. In addition, WGB shows an average accuracy drop of 0.57%, and RBOVG incurs 2.37%. WGLE is also robust to model post-processing techniques such as model pruning [24] or fine-tuning [25]. For example, WGLE maintains a false positive rate of zero under high pruning ratios, whereas RBOVG exhibits a false positive rate over zero, indicating that independently trained models are misidentified as unauthorized copies. WGLE enables the surrogate model to inherit the watermark from the original watermarked model, whereas WGB does not. Furthermore, WGLE requires only a 5% average computational overhead compared to RBOVG and 50% compared to WGB.

Contributions: We first consider the general scenario of watermark generation and embedding for WGLE: the owner has a large training graph and trains a GNN model on it (*Setting I*). We also discuss two other scenarios: the owner has the training graph and the GNN model, but the training

graph is small (*Setting II*). The owner has the original model but no training graph (*Setting III*).

Our contributions are summarized as follows:

- **Backdoor-free:** WGLE embeds the watermark by fine-tuning the original model to modify the LDDE values of selected edges in the trigger graph. WGLE eliminates security threats associated with backdoor attacks, as there is no incorrect mapping that causes specific samples to be misclassified into the designated class.
- **Multi-bit:** WGLE transforms the signs of the LDDE values of selected edges in the trigger graph to a multi-bit string (i.e. the watermark). Even if multiple watermarked models have been distributed, ownership verification requires only a single query to the suspect model. The single query makes the verification process financially inexpensive and difficult to detect. The multi-bit watermark is more difficult to forge than the zero-bit watermark.
- **Experiments:** We evaluated WGLE and state-of-the-art GNN copyright protection methods on six public datasets and six mainstream GNN architectures. The results demonstrate that WGLE ensures effectiveness and fidelity while addressing the limitations of existing methods.

II. BACKGROUND

A. Graph Neural Networks

GNNs are widely used in various graph data processing tasks. Since the challenges of black-box watermarking for node-level and graph-level GNNs differ, their solutions also vary. This paper focuses on node-level tasks under the inductive training paradigm like previous work [26], [27], [28].

In node-level GNNs, each node has a feature vector $\mathbf{x} \in \mathbf{X}$ and corresponding classification label $\mathbf{y} \in \mathbf{Y}$, where \mathbf{X} and \mathbf{Y} are the set of features and labels across all nodes, respectively. Let $\mathbf{G} = (\mathbf{X}, \mathbf{E})$ denote a graph with node feature set \mathbf{X} and edge set \mathbf{E} . A node-level GNN model takes \mathbf{G} as input and outputs predicted probability vectors for each node. GNN models create vector representations for individual nodes (embeddings) by iteratively gathering information from their local network neighborhoods. At each “layer” of the GNN models, a node’s new embedding is computed based on its current embedding and the embeddings of its immediate neighbors. This process is called neighborhood aggregation and message passing, where nodes exchange and combine information through the connecting edges. At the l -th layer, the embedding h_v^l of a node v is learned by iteratively aggregating the embeddings h_u^{l-1} of its neighboring nodes $u \in \mathcal{N}(v)$:

$$h_v^l = AGG(h_v^{l-1}, MSG(h_v^{l-1}, h_u^{l-1})), u \in \mathcal{N}(v),$$

where h_v^l is the embedding of node v at the l -th layer and h_v^0 is initialized by the node feature \mathbf{x} of node v . *MSG* stands for message aggregation, which calculates the messages exchanged between a node v and its neighbors u at layer $l-1$. These messages typically encapsulate information about local structural patterns and features. *AGG* is the aggregation function, which combines information from the previous layer’s

embedding h_v^{l-1} and the messages generated by the MSG function. Following k rounds of iteration, node embeddings at the k -th layer capture structural and feature information within their k -hop neighborhoods [29].

In practice, GNNs can follow two different training paradigms. In the transductive setting, the model is trained and evaluated on the same graph. In the inductive setting, it is trained on one graph and tested on another unseen graph. This work focuses on the inductive paradigm as it better reflects real-world deployment scenarios.

For graph data, edges are as important as features, influencing the accuracy and prediction behavior of GNN models. AGG and MSG in GNNs lead to the emergence of LDDE. The presence of LDDE implies that, in a black-box query, the GNN model can reveal not only the posterior probabilities of the samples but also the relationships between them. This allows ownership verification to depend on the prediction probabilities of the samples or the relationships between them. We further elaborate on LDDE in Section IV.

B. Model Ownership Verification

Model ownership verification determines whether the suspect model \mathcal{M}_s is an unauthorized copy of the protected model. It is formally defined as:

$$\mathcal{V}(\mathcal{M}_s, \text{IP}, \tau) = \mathbb{I}\{\text{SIM}(\text{IP}, \mathcal{F}_{\text{ext}}(\mathcal{M}_s)) > \tau\}$$

where IP denotes the predefined intellectual property (IP) identifier (e.g. watermark or fingerprint), $\mathcal{F}_{\text{ext}}(\cdot)$ is the extraction function, $\text{SIM}(\cdot, \cdot)$ is a similarity metric, and τ is the verification threshold. If the similarity exceeds τ , the model is considered to infringe the protected IP. We summarize the notation used in this work in Table I. Existing IP protection methods [30], [31], [32], [13], [16] can be categorized into three types: (1) white-box watermarking, (2) black-box watermarking, and (3) fingerprinting.

White-box watermarking. White-box watermarking methods directly encode a binary bit string into the internal parameters of a model. For example, Uchida et al. proposed adding a watermark regularization term to the loss function to embed the watermark [30]. White-box model watermarking methods assume that the verifier can have full access to the suspect model during verification. This assumption is often infeasible in practice, as models are commonly deployed as Machine Learning as a Service (MLaaS), where only the application programming interface (API) is exposed. Consequently, research on white-box watermarking has diminished, and no white-box watermarking schemes have been specifically designed for GNN models to date.

Black-box watermarking. Black-box watermarking methods assume that the verifier can only observe the outputs from the suspect model. Most methods [33], [31] rely on backdoor attacks. The backdoor is embedded into the model during training as a watermark. A backdoor refers to a hidden behavior activated by specific inputs, causing the model to produce predefined incorrect predictions, without impairing

TABLE I: Notations used in this work.

Notation	Description
$\mathbf{G} = (\mathbf{X}, \mathbf{E}, \mathbf{Y})$	Training graph
$\mathbf{T} = (\mathbf{X}, \mathbf{E})$	Trigger graph
\mathbf{X}	Set of node features
\mathbf{Y}	Set of node labels
\mathbf{E}	Set of edges
$\mathbf{E}_u/\mathbf{E}_v$	Nodes at the two ends of edges
\mathbf{w}	Watermark string
\mathbf{k}	Watermark key indicating selected edges
\mathbf{S}_w	Set of watermark strings
N_w	Number of bits in the watermark string \mathbf{w}
τ	Similarity threshold for verification
\mathcal{M}_o	Original model
\mathcal{M}_w	Watermarked model
\mathcal{M}_i	Independently trained model
\mathcal{M}_s	Suspect model for verification
\mathcal{F}_{LDDE}	Function for computing LDDE values

the model’s performance on benign data. Some methods use highly uncertain prediction samples as trigger samples to support fine-tuning embeddings [32]. To reduce backdoor harm, some methods use the specific entropy of the predictions as a watermark rather than incorrect class predictions [34]. During verification, the verifier inputs the triggers to the suspect model, where a high backdoor activation rate indicates an unauthorized copy [11], [12].

Fingerprinting. Fingerprinting constructs the fingerprint based on the intrinsic properties of the model, such as prediction behavior, decision boundaries, and responses to adversarial samples. Independently trained models exhibit distinct fingerprints, whereas an unauthorized copy shares a substantially similar fingerprint to the fingerprinted model. In the context of GNNs, fingerprints can take various forms, including layer-wise node embeddings [13], unique sample-specific behaviors [16], or overall model behaviors [14]. However, ownership verification based on fingerprint similarity results in a narrow collision space. After model post-processing, independently trained models may inadvertently generate fingerprints that resemble those of the protected model. This undermines the reliability of ownership verification.

III. PROBLEM STATEMENT

A. System and Threat Model

The system model of WGLE comprises three key entities: the original model owner, the adversary, and the verifier. The verifier can be a model owner or a trusted third-party authority qualified to issue legally admissible forensic reports.

Original Model Owner. The owner has the original GNN model, with or without the original training graph in practice. The owner’s objective is to embed a watermark into the original model with low overhead. For this purpose, the owner first constructs a single trigger graph based on the original model. For each distribution, a unique watermark string is generated that encodes metadata such as timestamps, recipient details, and usage agreements. The owner then uses

the trigger graph to fine-tune the original model to embed the watermark. Note that the trigger graph is reused across multiple distributions. Consequently, ownership verification requires only a single query using the same trigger graph, even if multiple watermarked models have been distributed.

Adversary. Two types of adversaries are considered:

- *IP Infringer.* The adversary has an unauthorized copy of the watermarked model. For example, the adversary can steal the entire model parameters through insider leaks or server breaches, or train a surrogate model via model extraction attacks. The adversary attempts to deploy the copy of the watermarked model to provide API access services while evading potential ownership verification. To evade ownership verification, the adversary can reprocess the watermarked model using techniques such as fine-tuning [25], pruning [24], or watermark overwriting [32].
- *Malicious User.* The watermark has been leaked and known to the adversary. In prior backdoor-based GNN black-box watermarking methods, such leakage directly reveals the backdoor and compromises the correct execution of the model on its primary task.

Verifier. Holding the trigger graph and the watermarks, the verifier aims to verify the ownership of the suspect model. In practice, ownership verification is typically performed in a black-box setting, where the verifier can only interact with the suspect model via its API. The verifier inputs the trigger graph into the suspect model and analyzes the output to determine whether the model is an unauthorized copy. If infringement is confirmed, the watermark can also reveal the source of the leak. As mentioned above, even if multiple watermarked models have been distributed, the verifier only needs to query the suspect model once using the trigger graph. The single query makes the verification process financially inexpensive and difficult to detect.

B. Requirements for Ownership Verification.

We propose WGLE, a novel GNN black-box watermarking paradigm that satisfies all the following requirements:

- R0. Effectiveness and Fidelity:** This is a fundamental requirement. Effectiveness requires that the scheme reliably distinguishes unauthorized copies from independently trained models. Fidelity requires that the watermarked model preserves a performance comparable to the original model on the primary task.
- R1. Backdoor-free:** The watermarked model is backdoor-free, eliminating the threat of backdoor attacks.
- R2. Multi-bit:** During ownership verification, the verifier extracts a multi-bit string (i.e., the watermark) from the suspect model. This allows the verification process to be financially inexpensive and less detectable. The watermark cannot be easily forged.
- R3. Robustness:** Ownership verification should remain effective even if the watermarked model is post-processed, such as pruning or fine-tuning.
- R4. Low Overhead:** The watermark embedding process incurs a low computational overhead.

TABLE II: Comparison of WGLE with previous methods. “**R1.**”, “**R2.**”, “**R3.**”, and “**R4.**” respectively denote backdoor-free, multi-bit, strong robustness, and low overhead. “●” denotes full compliance with the requirement, “○” indicates non-compliance, and “◐” represents partial fulfillment with room for improvement.

Category	Method	R1.	R2.	R3.	R4.
Fingerprinting	GrOVe [13]	●	○	○	○
	GNNFingers [16]	●	○	○	○
	RBOVG [14]	●	○	◐	○
Black-box watermarking	WGRG [11]	○	○	●	●
	WGB [12]	○	○	●	●
	WGLE	●	●	●	●

R0 is a basic requirement and must be addressed in all works. However, previous work has overlooked **R1-R4**, as discussed in Section III-C. In contrast, WGLE satisfies all the requirements outlined here.

C. Limitations of Prior Work

Table II compares WGLE with existing methods. However, previous works lack complete consideration of **R1**, **R2**, **R3**, and **R4** (introduced in Section III-B). We elaborate on the weaknesses of previous works as follows.

GNN Black-box Watermarking. WGRG [11] is the first GNN black-box watermarking method. WGB [12] further extends this line of work. They construct the backdoor samples by modifying the node features in node classification and modifying the graph topology in graph classification.

GNN black-box watermarking methods present strong robustness against model post-processing techniques (**R0**) and offer advantages in terms of overhead (**R4**). However, the integration of the backdoor introduces significant security vulnerabilities (**R1**), restricting their applicability in security-critical environments. Furthermore, these methods only possess zero-bit capacity. Ownership verification requires multiple queries to the suspect model, which increases financial cost and is prone to detection. In addition, the watermark is easily forged (**R2**) due to the prevalence of natural misclassifications. The adversary can collect many naturally misclassified samples to falsely claim ownership.

GNN Fingerprinting. GrOVe [13] is the first GNN fingerprinting method that utilizes layer-wise embedding entanglement for ownership verification. However, it requires access to intermediate layers, making it unsuitable for black-box settings. RBOVG [14] addresses this limitation and improves the robustness. They apply partial node feature masking and use the overall behavior of the model as the fingerprint to improve robustness. GNNFingers [16] can be applicable to tasks at various levels, including node-level, edge-level, and graph-level tasks. They jointly optimize the fingerprint and the ownership classifier. The classifier is trained to distinguish between the outputs of copied models (treated as positive samples) and those of independently trained models (treated as

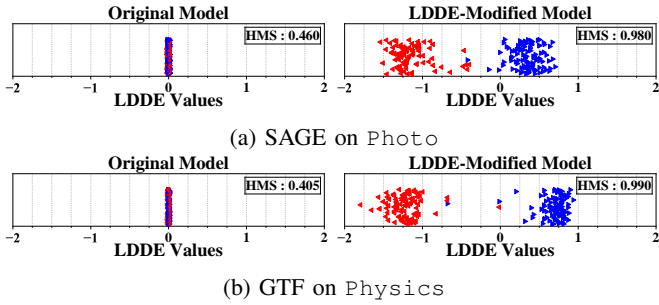


Fig. 1: Projections of LDDE values for selected edges before and after modification. Blue points represent edges targeted for positive LDDE signs, while red points represent those targeted for negative signs.

negative samples). The fingerprint is iteratively updated based on the classifier’s predictions.

GNN fingerprinting methods inherently avoid backdoors (R1). However, constructing fingerprints incurs high overhead (R4). It is prone to falsely identifying independently trained models as unauthorized copies if the models have undergone extensive post-processing. This compromises the credibility of ownership verification (R3). As a result, these methods are unsuitable for scenarios involving frequent model distribution or strict time constraints, as the fingerprints require much time to be reconstructed for each distributed model. Furthermore, model post-processing is routine in practice, and independently collected datasets are likely to exhibit overlap. Existing GNN fingerprinting methods only possess zero-bit capacity (R2).

IV. KEY INSIGHTS: LDDE

We begin by defining LDDE and then present three critical observations. These observations form our insight into the suitability of LDDE as a watermark carrier.

Definition IV.1. For two nodes (u, v) connected by an edge in the graph input to a GNN model, we define the difference between their node feature distance $\mathcal{D}(\mathbf{x}_u, \mathbf{x}_v)$ and their node prediction distance $\mathcal{D}(\hat{\mathbf{y}}_u, \hat{\mathbf{y}}_v)$ as LDDE, formally:

$$LDDE(u, v) = \mathcal{D}(\hat{\mathbf{y}}_u, \hat{\mathbf{y}}_v) - \mathcal{D}(\mathbf{x}_u, \mathbf{x}_v) \quad (1)$$

Here, we use cosine similarity for \mathcal{D} as it is bounded.

Observation-1. Given a graph with n edges as input to a GNN model, n LDDE values can be computed for the n edges. GNNs employ neighborhood aggregation and message-passing mechanisms to capture structural information from graph data [35]. These operations jointly leverage node features and graph topology, resulting in a predefined and measurable distance between connected nodes. Consequently, the LDDE value can be computed for every edge in any input graph to a GNN model.

Observation-2. LDDE values of certain edges can be modified to align their signs with predefined positive or negative signs. For example, to embed the watermark string “1001”, the owner selects four edges in the trigger graph that exhibit LDDE

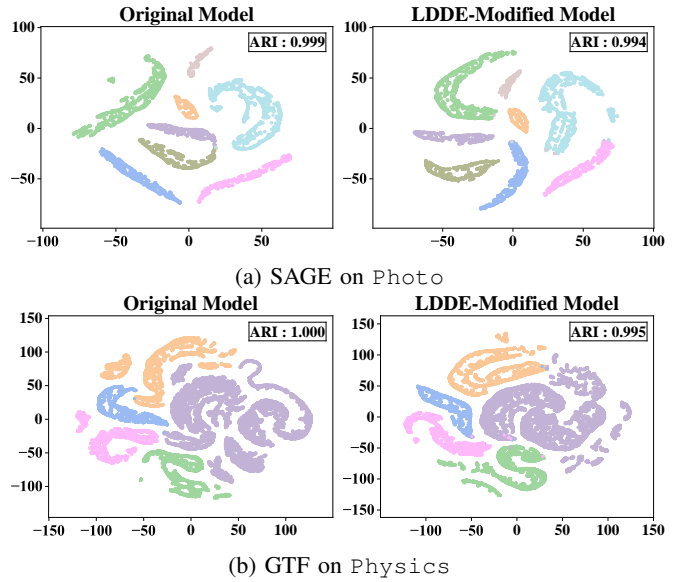


Fig. 2: t-SNE projections of the predictions from both the original and LDDE-modified (watermarked) models. Different colors indicate different classes.

values close to zero and possess rare local topologies. The original model is fine-tuned to jointly optimize two objectives: the primary task and the watermark embedding. The latter modifies the LDDE values of the selected edges to align their signs with “(+)(-)(-)(+)”, matching the watermark “1001”. The feasibility of simultaneously fitting multiple objectives has been established in previous work [36], [37].

We take *Setting 1* as an example, where the training graph is directly used as the trigger graph. In the experiment, a 200-bit string is randomly generated as the target watermark, with each bit corresponding to one of the 200 selected edges. The signs of the LDDE values for these edges are interpreted as the extracted watermark: a positive sign is assigned to bit “1”, and a negative sign to bit “0”. We compute the Hamming similarity (HMS) between the extracted bit string and the target watermark. In theory, the HMS for the original (unmodified) model should be close to 0.5, while the watermarked (LDDE-modified) model should yield a value approaching 1.0. As shown in Figure 1, the HMS increases from 0.460 to 0.980 for SAGE on Photo, and from 0.405 to 0.990 for GTF on Physics after modification. These results demonstrate that the LDDE values can be modified to encode the intended watermark. Additional results are presented in Appendix F.

Observation-3. Modifying the LDDE values of selected edges introduces a minor impact in the model’s primary task. In node-level GNNs, the distances between node pairs have been shown to correlate with the connectivity relationship: connected node pairs generally exhibit shorter distances than unconnected [38], [39]. As this relationship serves as auxiliary information that is not directly constrained by the model’s primary task, it allows for minor adjustments without noticeably degrading the model’s performance on the primary task.

We take *Setting I* as an example. Figure 2 shows the impact of the LDDE modification on the model’s performance in the primary task. Specifically, we calculate the Adjusted Rand Index (ARI) [40] on the node predictions in the training graph, before and after LDDE adjustment, to quantify the fitness of the model for the primary task. A smaller drop in ARI indicates minimal disruption to the primary task. As shown in Figure 2, both the original and watermarked models maintain high ARI scores. For example, ARI drops slightly from 0.999 to 0.994 for SAGE on `Photo`, and from 1.000 to 0.995 for GTF on `Physics`. These results confirm that LDDE modifications have a minor impact on the model’s primary task. Additional results are provided in Appendix F.

V. WGLE: DESIGN AND IMPLEMENTATION

We first discuss other potential implementation methods for achieving multi-bit or backdoor-free GNN model copyright protection. This section also introduces the specific settings of LDDE in this work. We then describe the general scenario (*Setting I*), where the owner has a large training graph and trains the original model on it. Subsequently, we consider two additional scenarios. *Setting II*: The owner has the training graph and trains the original model, but the training graph is small. *Setting III*: The ownership of the original model has been transferred to a new party that no longer has the original training graph. The new owner has to embed the watermark without the training graph. The notation used in this work is summarized in Table I.

A. Starwman Solutions

A straightforward solution is to directly adopt black-box watermarking methods for models processing Euclidean data to GNN ownership verification. However, such methods are not well-suited to GNNs due to the complex and irregular nature of graph data. For example, UBW [37] uses a specific entropy value as a watermark. Trigger samples output correct classifications while exhibiting unusually high entropy. However, UBW substantially alters the sample output, severely degrading fidelity and increasing the likelihood of ownership misidentification for GNNs. In node-level GNNs, a node’s prediction is determined by the features of both itself and its neighbors. Thus, altering the output of a single node can affect a large number of surrounding nodes. EaaW [41] proposes a multi-bit black-box watermarking method by transforming the explanation of a specific trigger sample into the watermark. However, due to the non-Euclidean nature of graph data, EaaW struggles with issues of fidelity and effectiveness (as presented in Section VI). To overcome these issues, we explore GNN-specific properties for GNN black-box watermarking.

Previous studies [38], [39] show that the distance between a pair of nodes can reveal the existence of an edge. With the same GNN model, a pair of nodes with or without an edge yields different output distances. Inspired by this observation, we fix the input graph and make different watermarked GNN models produce distinct node output distances. A straightforward idea is to assign specific values to the output distances of

the connected nodes. However, GNN black-box watermarking must consider (1) selecting a suitable distance metric, (2) mapping node distances to watermark bits, and (3) coping with the output form of the suspect model.

For these considers (1) we adopt cosine similarity as the distance metric in LDDE, as cosine similarity is bounded within $[-1, 1]$; (2) we map the signs of LDDE values into a watermark string, where positive signs correspond to “1” and negative signs correspond to “0”. We do not directly use the distance of the node outputs, as it does not guarantee a sufficient number of values near zero; and (3) we applied a transformation to the posterior probabilities before calculating LDDE [42], since GNNs deployed via MLaaS typically return softmax-normalized probability distributions. Specifically, for node predictions $\hat{\mathbf{Y}}$, node features \mathbf{X} and edges \mathbf{E} , we define the LDDE function as follows:

$$\mathcal{F}_{LDDE}(\hat{\mathbf{Y}}, \mathbf{X}, \mathbf{E}) = \mathcal{D}(\tilde{\mathbf{Y}}_{\mathbf{E}_u}, \tilde{\mathbf{Y}}_{\mathbf{E}_v}) - \mathcal{D}(\mathbf{X}_{\mathbf{E}_u}, \mathbf{X}_{\mathbf{E}_v}) \quad (2)$$

where $\mathbf{E}_u/\mathbf{E}_v$ denotes the nodes at the two ends of \mathbf{E} , $\mathcal{D}(\cdot)$ is cosine similarity, and $\tilde{\mathbf{Y}}$ represents a transformation of a node prediction $\hat{\mathbf{Y}}$, which is

$$\tilde{\mathbf{Y}} = \frac{\log(\hat{\mathbf{Y}}) - \mu(\log(\hat{\mathbf{Y}}))}{\sigma(\log(\hat{\mathbf{Y}}))},$$

where \log is natural logarithms; μ is the mean; σ is the standard deviation. μ and σ are calculated over dimensions for each sample. This transformation addresses the issue of posterior probabilities being small and closely spaced (i.e., within the range of 0 to 1), which are unsuitable for cosine similarity computation.

B. Setting I: Large Training Graph

In most cases, the training graph consists of many nodes and edges, which can thus serve directly as the trigger graph. This strategy provides excellent concealment during ownership verification and robustness against model extraction attacks, as the trigger graph is the unmodified training graph.

Watermark Generation: As illustrated in Figure 3, the watermark generation process begins by calculating the LDDE values for all edges in the trigger graph and selecting a subset of edges that are marked by the watermark key. Note that both the LDDE values and the watermark key are computed once and reused across all watermarked models. For each distribution, a distinct watermark string is generated according to practical requirements.

The watermark string encodes the desired information, such as the company logo, the usage policy associated with the watermarked model, the intended recipient of the model distribution, or a timestamp indicating when the model was distributed. In this work, we generate an N_w -bit watermark string by independently sampling each bit from a Bernoulli distribution with equal probability for 0 and 1 (i.e., Bernoulli(0.5)).

$$\mathbf{w} = (w_1, w_2, \dots, w_{N_w}), \quad w_i \sim \text{Bernoulli}(0.5) \quad (3)$$

In fact, the watermark string can encode arbitrary information.

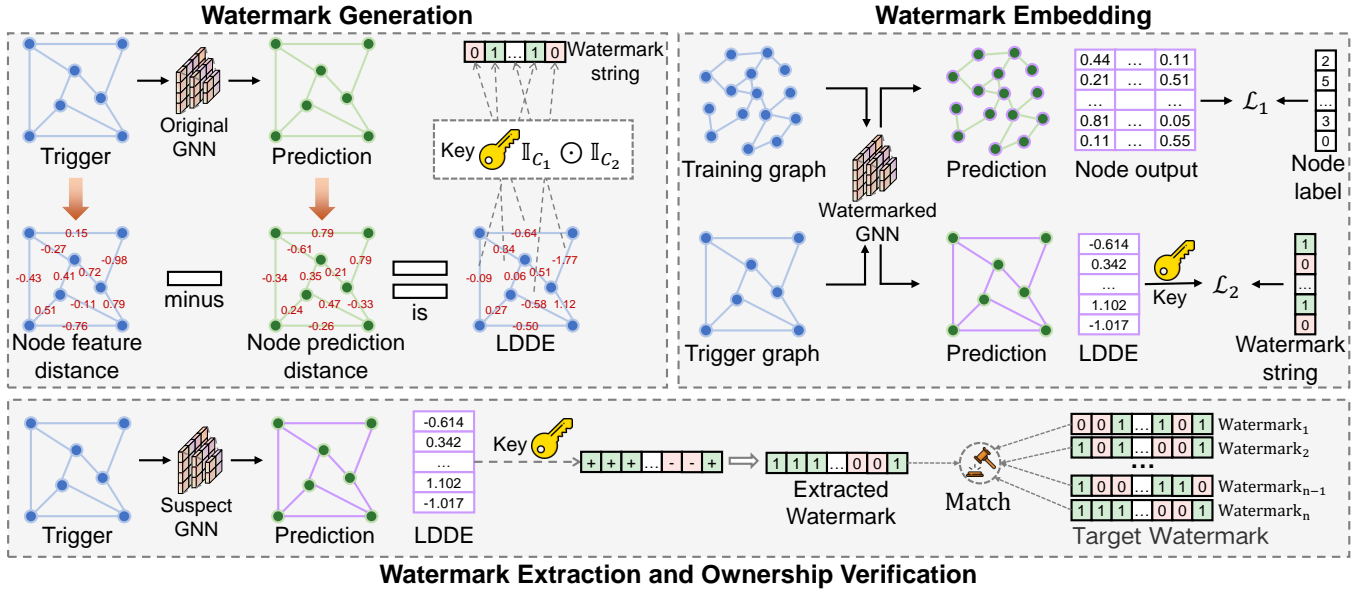


Fig. 3: The main pipeline of WGLE. The trigger graph and the watermark key are prepared for the original model. For each distribution, the model is fine-tuned to be embedded the given watermark. During fine-tuning, the primary task is preserved by the training graph, while the watermark string is embedded via the trigger graph. During ownership verification, the trigger graph is used to query the suspect model’s API, and the watermark is extracted from its LDDE values.

Although every edge possesses an LDDE value, not all edges are suitable as watermark carriers. The edges selected to carry the watermark should satisfy the following conditions.

- C1:** *The edges possess statistically rare local structures.*
- C2:** *The edges possess LDDE values close to zero.*

Edges that better satisfy condition **C1** minimize the impact of modifying LDDE values on other edges. Edges that better satisfy condition **C2** require smaller adjustments to alter the signs of their LDDE values. We use the watermark key \mathbf{k} to indicate the selected edges in the trigger graph that are used to carry the watermark string.

Using the Training Graph as the Trigger Graph. When using the training graph \mathbf{G} as the trigger graph \mathbf{T} , condition **C1** can be satisfied by selecting edges that connect nodes with different labels. Since nodes connected in a graph tend to share the same label, such edges connecting nodes with different labels exhibit a rare local topology. To satisfy condition **C2**, the LDDE values of the edges that satisfy condition **C1** are calculated, and the N_w edges with the smallest absolute LDDE values are selected.

Watermark Embedding: As illustrated in Figure 3, the original model owner maintains the performance of the watermarked model \mathcal{M}_w in the primary task by the training graph \mathbf{G} while embedding the watermark string \mathbf{w} by the trigger graph \mathbf{T} and the watermark key \mathbf{k} . The owner fine-tunes the original model \mathcal{M}_o to optimize the following objective function until \mathbf{w} is successfully extracted from \mathcal{M}_w :

$$\min_{\mathcal{M}_w} \mathcal{L} = \mathcal{L}_1(\mathcal{M}_w(\mathbf{G}), \mathbf{G} \cdot \mathbf{Y}) + \mathcal{L}_2(\mathbf{v}[\mathbf{k}], \mathbf{w}) \quad (4)$$

where \mathcal{L}_1 represents the cross-entropy loss for the primary task. \mathcal{L}_2 measures the dissimilarity between the extracted watermark string and \mathbf{w} , which is the binary cross-entropy loss in this work. \mathcal{M}_w is the watermarked model, initialized as \mathcal{M}_o . $\mathbf{v} = \mathcal{F}_{LDDE}(\mathcal{M}_w(\mathbf{T}), \mathbf{T} \cdot \mathbf{X}, \mathbf{T} \cdot \mathbf{E})$ denotes the vector of LDDE values for all edges. \mathbf{k} is the watermark key that indicates the selected edges.

Watermark Extraction and Ownership Verification: As shown in Figure 3, the verifier queries the suspect model’s API using the trigger graph to obtain the predictions for all nodes. The verifier then computes the LDDE values for all edges and selects a subset according to the watermark key to form a sequence. This sequence is binarized to recover the embedded watermark. The complete extraction procedure is detailed in Algorithm 1.

$\text{Signal}(x)$ returns 0 if $x < 0$ and 1 otherwise. SIM stands for similarity. τ is the judgment threshold and can be selected according to the normal distribution. Note that if the suspect model is an unauthorized copy, the return is the original watermark in \mathbf{S}_w , not the extracted one. We provide a detailed discussion of the selection of τ in Appendix D.

C. Setting II: Small Training Graph.

Setting I utilizes the training graph \mathbf{G} as the trigger graph \mathbf{T} , which requires \mathbf{G} to be large enough to contain enough edges that satisfy conditions **C1** and **C2**. However, in real-world scenarios, \mathbf{G} may be too small to contain enough edges that satisfy these conditions. In this case, the owner has to generate a graph to serve as the trigger graph. The key distinction between *Setting I* and *Setting II* lies in the generation of \mathbf{T} , while other components remain unchanged.

Algorithm 1: Ownership Verification

Input : API of the suspect model \mathcal{M}_s ; Trigger graph \mathbf{T} ; Watermark Key \mathbf{k} ; Watermark set $\mathbf{S}_w = \{\mathbf{w}_i\}_{i=1}^n$;
Output: (1) A boolean value: True if \mathcal{M}_s is identified as an unauthorized copy; (2) The matched watermark string, returned only if True.

- 1 $\hat{\mathbf{Y}} \leftarrow \mathcal{M}_s(\mathbf{T})$;
- 2 $\mathbf{v} \leftarrow \mathcal{F}_{LDDE}(\hat{\mathbf{Y}}, \mathbf{T}, \mathbf{X}, \mathbf{T}, \mathbf{E})$;
- 3 $\tilde{\mathbf{w}} \leftarrow \text{Signal}(\mathbf{v}[\mathbf{k}])$;
- 4 $\mathbf{w}_m \leftarrow \arg \max \text{SIM}(\tilde{\mathbf{w}}, \mathbf{S}_w)$;
// $\mathbf{w}_m \in \mathbf{S}_w$ is the most similar watermark to $\tilde{\mathbf{w}}$
- 5 **if** $\text{SIM}(\mathbf{w}_m, \tilde{\mathbf{w}}) \geq \tau$ **then return** True, \mathbf{w}_m ;
- 6 **else return** False;

Using the Generated Graph as the Trigger Graph. The trigger graph topology can be generated using the Erdos-Renyi (ER) model [11] or borrowed from a real graph for better concealment. We adopt the topology of PubMed[43] as the trigger graph structure in this work. The initial node features are randomly sampled from a Gaussian distribution, with feature dimensions matching those of the training graph. These features are then updated to satisfy the following objectives:

$$\min_{\mathbf{T}, \mathbf{X}} \mathcal{L} = |\mathbf{v}| + \lambda_1 \cdot \frac{1}{1 - |\mathcal{D}(\mathbf{T}, \mathbf{X}_{\mathbf{T}, \mathbf{E}_w}, \mathbf{T}, \mathbf{X}_{\mathbf{T}, \mathbf{E}_v})|} \quad (5)$$

\mathbf{v} is $\mathcal{F}_{LDDE}(\mathcal{M}_o(\mathbf{T}), \mathbf{T}, \mathbf{X}, \mathbf{T}, \mathbf{E})$, which minimizes the absolute value of LDDE values across all edges. The second term imposes a penalty to prevent node feature distances from approaching the boundaries of the cosine similarity range $[-1, +1]$. This is because when the node feature distance approaches the cosine similarity boundary, it becomes difficult to flip the signs of the LDDE values, even if the values are close to zero. λ_1 is a regularization coefficient, which is $1e-4$ in this work. After completion of the updates, we applied Node2Vec [44] and DBSCAN [45] to identify edges that meet the condition **C1** due to the absence of labels. Subsequently, we select N_w edges that meet condition **C2**.

Setting II is suitable for scenarios where the training graph \mathbf{G} is small. Compared to *Setting I*, it imposes a smaller impact on the fidelity of the model. However, since *Setting II* relies on a generated trigger graph \mathbf{T} rather than the original training graph, it makes the watermarked model \mathcal{M}_w not robust against model extraction attacks.

D. Setting III: No Training Graph.

Both *Setting I* and *Setting II* require the training graph \mathbf{G} to maintain the performance of the watermarked model \mathcal{M}_w on the primary task. However, the lack of \mathbf{G} is common in real-world scenarios. For example, the owner trains a model and then releases it to a platform or publisher. To protect data privacy, the owner provides the model without \mathbf{G} . If the platform or publisher wants to embed a watermark in the

model, they face the challenge of lacking \mathbf{G} to maintain the performance of \mathcal{M}_w on the primary task. *Setting III* is suitable for the scenario where \mathbf{G} is not available. The key distinction between *Setting II* and *Setting III* lies in the watermark embedding, while other components remain unchanged.

Watermark Embedding without the Training Graph. In the absence of \mathbf{G} , the challenge during watermark embedding lies in maintaining the performance of \mathcal{M}_w in the primary task. To address this, we adapt the concept of data-free adversarial distillation (DFAD) for GNNs [46], [47]. Specifically, we adopt the Barabasi-Albert (BA) model [48] to randomly generate the pseudo graph topology $\tilde{\mathbf{G}}, \mathbf{E}$, and initialize the node features $\tilde{\mathbf{G}}, \mathbf{X}$ with samples drawn from a Gaussian distribution. $\tilde{\mathbf{G}}$ acts as a substitute for \mathbf{G} . During watermark embedding, after each update to \mathcal{M}_w , $\tilde{\mathbf{G}}, \mathbf{X}$ is updated to maximize the output difference between the original model \mathcal{M}_o and the watermarked model \mathcal{M}_w . The optimization objective is:

$$\min_{\mathcal{M}_w} \max_{\tilde{\mathbf{G}}, \mathbf{X}} \mathcal{L} = \mathcal{L}_1(\mathcal{M}_w(\tilde{\mathbf{G}}), \mathcal{M}_o(\tilde{\mathbf{G}})) + \mathcal{L}_2(\mathbf{v}[\mathbf{k}], \mathbf{w}) \quad (6)$$

where \mathcal{L}_1 represents the cross-entropy loss for the primary task. \mathcal{L}_2 measures the dissimilarity between the extracted watermark string and \mathbf{w} , which is the binary cross-entropy loss in this work. \mathcal{M}_w is the watermarked model, initialized as \mathcal{M}_o . $\mathbf{v} = \mathcal{F}_{LDDE}(\mathcal{M}_w(\mathbf{T}), \mathbf{T}, \mathbf{X}, \mathbf{T}, \mathbf{E})$ denotes the vector of LDDE values for all edges. \mathbf{k} is the watermark key that indicates the selected edges.

Unlike classical DFAD for GNNs [47], which updates both the node features and the graph topology, *Setting III* keeps the graph topology fixed and updates only the node features. This is because LDDE is relevant to the graph topology, and altering the topology would increase the uncertainty of modifying the LDDE values. The principle of *Setting III* is that the optimal points of the watermarked model and the original model are very close, enabling the original model to be transformed into the watermarked model with minor alteration.

VI. EXPERIMENTS

We evaluated WGLE in six real-world datasets and six mainstream model architectures. We first describe the experimental setting and then demonstrate the experimental results.

A. Experiments Setting

Environment. We conducted the experiments on a cloud server using an NVIDIA A100 GPU with 40GB RAM. We used PyTorch 2.5.1 and PyG 2.6.1 as the programming languages for our experiments.

Dataset. We used the six datasets as shown in Table III for our experiments. Each dataset is represented as a graph, where each node corresponds to a sample. For each graph, i.e., a dataset, we extract 70% of the nodes and their connected edges as the training graph, 20% of the nodes and their connected edges as the validation graph, and 10% of the nodes and their connected edges as the test graph.

Model Architectures We used GCNv2 [51], Graph Transformer (GTF)[52], GraphSAGE [53], SSG [54], GEN [55], and ARMA[56] in our experiments. Except for GCNv2, each

TABLE III: Datasets statistics of node classification task

Datasets	Nodes	Edges	Features	Classes
Cora [43]	2,708	10,556	1,433	7
DBLP [49]	17,716	105,734	1,639	4
Photo [50]	7,650	238,162	745	8
Computers [50]	13,752	491,722	767	10
CS [50]	18,333	163,788	6,805	15
Physics [50]	34,493	495,924	8,415	5

architecture includes four graph convolution layers, with the final layer serving as the output layer. GCNv2 is composed of an input linear layer, three graph convolution layers, and an output linear layer. All models use the ELU activation function, with the Adam optimizer set to a learning rate of 1e-4 and a weight decay of 1e-4. Each model is trained for 500 iterations, and we use the cross-entropy loss as the objective function for the primary tasks.

Metrics. We use following metrics to evaluate WGLE:

- *Test Accuracy (TAC)*: The accuracy of the model on the test graph, expressed as a percentage in this paper.
- *Hamming similarity (HMS)*: Hamming similarity quantifies the similarity between two binary strings of equal length. Formally, given two binary sequences $\tilde{\mathbf{w}}, \mathbf{w} \in \{0, 1\}^{N_w}$, the HMS is defined as:

$$\text{HMS}(\tilde{\mathbf{w}}, \mathbf{w}) = \frac{1}{N_w} \sum_{i=1}^{N_w} \mathbb{I}\{\tilde{\mathbf{w}}[i] = \mathbf{w}[i]\} \quad (7)$$

where $\mathbb{I}(x)$ is an indicator function that returns 1 if x is true and 0 otherwise. $\tilde{\mathbf{w}}$ is the extracted watermark string, while \mathbf{w} is the target watermark string. N_w is the length of the watermark string. HMS ranges from 0 to 1, with 1 indicating perfect agreement and 0.5 meaning random guessing.

- *Ownership Verification Accuracy (OVA)*: Correct detection rate of ownership verification.
- *False Positive Rate (FPR)*: FPR reports the rate of independently trained models mistakenly identified as unauthorized copies. It must remain zero; any value above zero indicates that the ownership verification audit is untrustworthy.

We adopted the midpoint of each similarity metric as the decision threshold τ : A similarity score over τ indicates an unauthorized copy. Specifically, τ is set to 0.5 for WGB (backdoor activation rate), 0.5 for RBOVG (confidence score of the ownership classifier), and 0.75 for WGLE and EaaW (hamming similarity). A detailed discussion on the relationship between similarity thresholds and ownership collisions is provided in Appendix D.

Baseline. We select WGB [12] and RBOVG [14] as baselines for comparison. These methods represent the state-of-the-art in GNN black-box watermarking and GNN fingerprinting, respectively. We simultaneously tested whether EaaW [41] can be directly transplanted to GNN.

Empirical Evaluations. We conduct comprehensive experiments to address the following research questions (RQs):

- RQ1. Compared to baselines, can WGLE effectively distinguish watermarked models and independently trained

models, achieving high ownership verification accuracy (OVA) and a zero false positive rate (FPR) (effectiveness)? In addition, to what extent does watermarking affect the model’s accuracy in the primary task (fidelity)?

- RQ2. Can ownership verification remain effective when watermarked models or independently trained models are subjected to common post-processing techniques such as fine-tuning or pruning?
- RQ3. Can ownership verification remain reliable even if the adversary is aware of the WGLE algorithm and adopts targeted countermeasures (watermark overwriting)? Can the watermark be extracted from a surrogate model that is trained via model extraction attacks?

We systematically answer these RQs. Moreover, we show the overhead of watermark embedding in Appendix B, the harm of the backdoor in Appendix C, the analysis of ownership collision in Appendix D, and the impact of watermark length on fidelity and robustness in Appendix E.

B. Effectiveness and Fidelity (RQ1)

Experiment Design. We fine-tune the original model to embed the watermark using the Adam optimizer with a learning rate of 5e-5 and a weight decay of 1e-4. The length of the watermark string N_w is 200. We generated 100 watermarked models and 100 independently trained models. For WGB, we mask 15% of node features and assign the label “2” to create backdoor samples. For RBOVG, we follow the authors’ default settings, training 60 shadow surrogate models and 60 independently trained models. The training graph is evenly split: one half is used to train fingerprinted models and the other to train shadow models. Consequently, only half of the training graph is available for training the fingerprinted model. The other settings are consistent for a fair comparison.

Result Analysis. As shown in Table IV, WGLE, WGB, and RBOVG effectively distinguish watermarked or fingerprinted models from independently trained models. All three methods achieve an OVA of 1.000 and no FPR over 0, reflecting perfect discrimination without incorrect identifications. In contrast, EaaW fails to achieve perfect classification, with OVA scores below 1.0 in all datasets and models, and even exhibiting FPR values greater than 0 for SSG on DBLP and GEN on CS. These results indicate that, despite its effectiveness in image and text domains, EaaW is not well-suitable for GNN watermarking.

Table V reports the results of the fidelity. WGLE under *Settings II* and *Settings III* achieves minimal accuracy degradation, with maximum drops of 1.52% and 1.85%, respectively. This is attributed to using a generated graph as the trigger graph. *Settings I* shows better fidelity than RBOVG but worse than WGB, with a maximum drop of 5.82%. The large drop is due to the small size of the training graph of Cora, which limits the model to fit both the primary task and the watermark embedding task. Therefore, when the training graph is small and the watermark string is long, *Settings I* should be carefully considered if high fidelity is required. In contrast, EaaW incurs a maximum accuracy drop of 12.77% on the test graph.

TABLE IV: The effectiveness of WGLE and baselines. We report the ownership verification accuracy (OVA) and the false positive rate (FPR).

Datasets	Models	WGB		RBOVG		EaaW		Setting I		Setting II		Setting III	
		OVA	FPR	OVA	FPR	OVA	FPR	OVA	FPR	OVA	FPR	OVA	FPR
Cora	GCNv2	1.000	0.000	1.000	0.000	0.891	0.000	1.000	0.000	1.000	0.000	1.000	0.000
DBLP	SSG	1.000	0.000	1.000	0.000	0.547	0.031	1.000	0.000	1.000	0.000	1.000	0.000
Photo	SAGE	1.000	0.000	1.000	0.000	0.984	0.000	1.000	0.000	1.000	0.000	1.000	0.000
Computers	ARMA	1.000	0.000	1.000	0.000	0.969	0.000	1.000	0.000	1.000	0.000	1.000	0.000
CS	GEN	1.000	0.000	1.000	0.000	0.969	0.031	1.000	0.000	1.000	0.000	1.000	0.000
Physics	GTF	1.000	0.000	1.000	0.000	0.875	0.000	1.000	0.000	1.000	0.000	1.000	0.000

TABLE V: The test accuracy (TAC) of the original model (\mathcal{M}_o) and the watermarked or fingerprinted models in WGB, RBOVG, EaaW, and WGLE. Values following \pm denote the standard deviation (unbiased estimate), and the values following $\uparrow\downarrow$ indicate the relative decrease or increase in TAC compared to \mathcal{M}_o .

Datasets	Models	\mathcal{M}_o	WGB	RBOVG	EaaW	Setting I	Setting II	Setting III
Cora	GCNv2	73.16	74.81 \pm 1.44 \uparrow 1.65	69.61 \pm 0.86 \downarrow 3.55	60.39 \pm 1.04 \downarrow 12.77	67.34 \pm 2.14 \downarrow 5.82	72.91 \pm 0.98 \downarrow 0.25	73.14 \pm 0.92 \downarrow 0.02
DBLP	SSG	72.01	71.92 \pm 0.52 \downarrow 0.09	64.37 \pm 0.31 \downarrow 7.64	70.98 \pm 0.36 \downarrow 1.03	70.05 \pm 0.75 \downarrow 1.96	71.93 \pm 0.34 \downarrow 0.08	71.94 \pm 0.33 \downarrow 0.07
Photo	SAGE	87.97	85.67 \pm 0.85 \downarrow 2.30	85.81 \pm 0.73 \downarrow 2.16	86.68 \pm 0.65 \downarrow 1.29	84.98 \pm 0.87 \downarrow 2.99	86.45 \pm 0.56 \downarrow 1.52	86.12 \pm 0.60 \downarrow 1.85
Computers	ARMA	82.84	80.19 \pm 0.71 \downarrow 2.65	83.53 \pm 0.92 \uparrow 0.69	75.76 \pm 0.64 \downarrow 7.08	80.82 \pm 0.64 \downarrow 2.02	82.40 \pm 0.38 \downarrow 0.44	82.49 \pm 0.36 \downarrow 0.35
CS	GEN	90.02	89.92 \pm 0.69 \downarrow 0.10	89.16 \pm 0.25 \downarrow 0.86	84.35 \pm 0.33 \downarrow 5.67	90.48 \pm 0.40 \uparrow 0.46	90.65 \pm 0.22 \uparrow 0.63	90.67 \pm 0.23 \uparrow 0.65
Physics	GTF	92.84	92.87 \pm 0.42 \uparrow 0.03	92.07 \pm 0.17 \downarrow 0.77	87.63 \pm 0.20 \downarrow 5.21	92.57 \pm 0.26 \downarrow 0.27	92.82 \pm 0.12 \downarrow 0.02	92.80 \pm 0.09 \downarrow 0.04

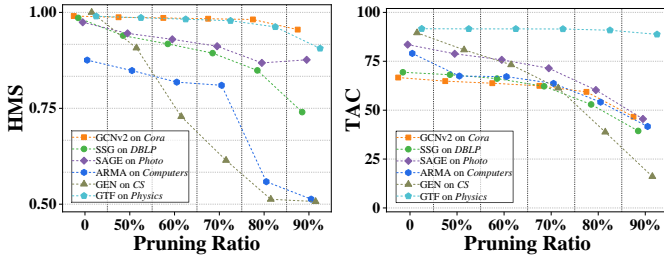


Fig. 4: Hamming similarity (HMS) and test accuracy (TAC) of watermarked models against model pruning in *Setting I*.

Answers to RQ1: WGLE achieves perfect accuracy (100%) in ownership verification. Regarding fidelity, assessed through average accuracy degradation, the performance ranking is: *Setting II* (0.28) \approx *Setting III* (0.28) < WGB (0.57) < *Setting I* (2.1) \approx RBOVG (2.38) < EaaW (5.51).

C. The Robustness against Fine-tuning and Pruning (RQ2)

Experiment Design. Pruning and fine-tuning are widely adopted post-processing techniques [14], [15]. Pruning removes parameters with minimal contributions to the model’s primary task to reduce the complexity of the model, while fine-tuning retrains the model on a small dataset to improve performance. They may disrupt the embedded watermark as they alter the output distribution of the watermarked model. The specific experimental settings are as follows:

- Pruning: The adversary performs L1-norm pruning by zeroing out the neurons with the smallest L1 norms. We report changes in HMS and TAC as the pruning ratio increases from 0% to 50%, 60%, 70%, 80%, and 90%.
- Fine-tuning: The adversary fine-tunes the watermarked model on the validation graph using the Adam optimizer with a learning rate of $5e-5$ (identical to that used during

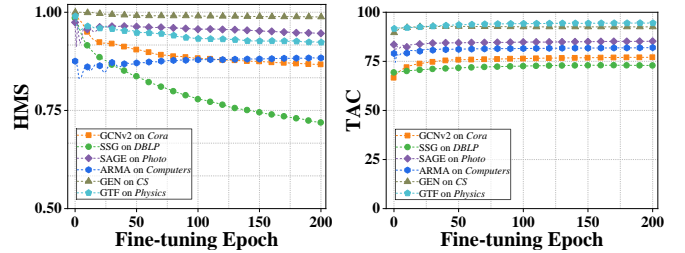


Fig. 5: Hamming similarity (HMS) and test accuracy (TAC) of watermarked models against fine-tuning in *Setting I*.

watermark embedding). We report the variations in HMS and TAC as the number of fine-tuning epochs increases.

- Ownership collision is an essential consideration in reliable watermark verification. Independently trained models may undergo pruning or fine-tuning for non-malicious purposes. We apply pruning and fine-tuning to independently trained models and evaluate whether false positives occur during ownership verification.

We present the changes in TAC and HMS of the watermarked models as the pruning ratio increases and the number of fine-tuning epochs grows. We also compare the OVA and FPR of WGLE with those of the baselines under specific pruning ratios and after fine-tuning with 200 epochs.

Result Analysis. Figure 4 illustrates the impact of various pruning ratios on HMS and TAC under *Setting I* of WGLE. In general, both metrics degrade as the pruning ratio increases. Among all models, GEN on CS exhibits the weakest robustness, where the HMS falls below the verification threshold with a pruning ratio of 60%. However, its TAC simultaneously drops to around 60%, indicating that the model becomes practically unusable. In contrast, SAGE on Photo demonstrates the highest robustness: even at a pruning ratio of 90%, where

TABLE VI: Ownership verification accuracy (OVA) and false positive rate (FPR) of WGLE, WGB, and RBOVG after pruning the independently trained models. The pruning ratio is determined when RBOVG first exhibits a non-zero FPR.

Datasets	Models	Pruning Ratio	WGB		RBOVG		Setting I		Setting II		Setting III	
			OVA	FPR	OVA	FPR	OVA	FPR	OVA	FPR	OVA	FPR
Cora	GCNv2	70%	1.000	0.000	0.855	0.180	1.000	0.000	1.000	0.000	1.000	0.000
DBLP	SSG	80%	0.500	0.000	0.725	0.550	1.000	0.000	1.000	0.000	0.990	0.000
Photo	SAGE	70%	1.000	0.000	0.875	0.250	1.000	0.000	1.000	0.000	1.000	0.000
Computers	ARMA	50%	0.990	0.000	0.890	0.220	0.990	0.000	1.000	0.000	1.000	0.000
CS	GEN	70%	0.855	0.000	0.680	0.640	0.510	0.000	0.500	0.000	0.500	0.000
Physics	GTF	60%	1.000	0.000	0.925	0.150	1.000	0.000	1.000	0.000	1.000	0.000

TABLE VII: Ownership verification accuracy (OVA) and false positive rate (FPR) of WGLE, WGB, and RBOVG when the independently trained models are fine-tuned with 200 epochs.

Datasets	Models	WGB		RBOVG		Setting I		Setting II		Setting III	
		OVA	FPR	OVA	FPR	OVA	FPR	OVA	FPR	OVA	FPR
Cora	GCNv2	0.630	0.000	1.000	0.000	0.980	0.000	1.000	0.000	1.000	0.000
DBLP	SSG	0.990	0.000	1.000	0.000	0.582	0.000	1.000	0.000	1.000	0.000
Photo	SAGE	0.965	0.000	1.000	0.000	1.000	0.000	1.000	0.000	1.000	0.000
Computers	ARMA	0.700	0.000	0.925	0.150	1.000	0.000	1.000	0.000	1.000	0.000
CS	GEN	1.000	0.000	0.735	0.020	1.000	0.000	1.000	0.000	1.000	0.000
Physics	GTF	1.000	0.000	1.000	0.000	1.000	0.000	1.000	0.000	1.000	0.000

TAC falls below 50%, HMS remains above 0.8.

Figure 5 presents HMS degradation as increasing fine-tuning epochs. In most cases, HMS exhibits minor fluctuations at the beginning and then stabilizes. An exception is SSG on DBLP, where the HMS consistently decreases and eventually fails to meet the ownership verification threshold after 200 epochs of fine-tuning. For all other models, HMS remains stable, showing strong resilience to fine-tuning.

Table VI presents the ownership verification accuracy (OVA) and the false positive rate (FPR) in specific pruning ratios. We take the pruning ratio at which RBOVG first incurs false positives as a baseline and report the corresponding OVA and FPR for WGLE and WGB. WGLE consistently demonstrates higher robustness than RBOVG. For example, for GCNv2 on Cora and SSG on DBLP, the three settings of WGLE achieve 100% OVA without false positives, while RBOVG fails to verify ownership and its FPR over zero. WGB and WGLE exhibit similar levels of robustness.

Most importantly, WGLE maintains an FPR of zero in all cases, ensuring that independently trained models are never mistakenly identified as unauthorized copies. In contrast, RBOVG exhibits nonzero FPR in specific pruning ratios, meaning it misclassifies benign models as infringements. An FPR greater than zero undermines the credibility of ownership audits. Alarmingly, the probability of ownership collision cannot be known in RBOVG. We analyze how the probability of ownership collision can be influenced by the similarity threshold and watermark length in Appendix D.

Table VII shows the results after fine-tuning the independently trained models on the validation graph with 200 epochs. We observe that the *Setting II* and *Setting III* of WGLE demonstrate strong robustness against fine-tuning. *Setting I* and RBOVG each show strengths in different models, but both outperform WGB. Importantly, we emphasize that the FPR of RBOVG

is not zero in certain cases. As discussed earlier, any false positive rate above zero can compromise the credibility of the ownership verification process.

Answers to RQ2: The adversary cannot remove the watermark without incurring a substantial drop in the test accuracy of the watermarked model. For example, to reduce the HMS of the watermark below 0.75 by pruning to disable ownership verification, the test accuracy of the watermarked model on the primary task (GEN on CS) degraded by 15%, which is unacceptable in practice. In contrast, WGLE produces no false positives for independently trained models, even if they are post-processed by pruning or fine-tuning.

D. Robustness against Watermark Overwriting and Model Extraction Attacks (RQ3)

Experiment Design. *Setting III* of WGLE allows watermark embedding without the original training graph. The adversary attempts to embed a new watermark in the watermarked model to potentially overwrite the original watermark. Model extraction attacks refer to the adversary training a local surrogate model by querying the API of the watermarked model. The surrogate model may replicate the functionality of the watermarked model without inheriting the embedded watermark. The specific experimental settings are as follows:

- **Overwriting:** The adversary generates a trigger graph using the topology of CiteSeer and embeds a new watermark in the watermarked model by *Setting III* of WGLE. We report the HMS and TAC of the original watermark before and after watermark overwriting.
- **Model extraction attacks:** The adversary has 80% of the nodes in the training graph, along with the edges among them, but without the corresponding labels. These samples and edges are used to query the watermarked model and obtain the corresponding prediction probabilities. The ad-

TABLE VIII: Test accuracy (TAC) and hamming similarity (HMS) of watermarked models (\mathcal{M}_w) before and after overwriting. Values before and after \rightarrow indicate the metrics before and after overwriting, respectively.

Datasets	Models	<i>Setting I</i>		<i>Setting II</i>		<i>Setting III</i>	
		TAC	HMS	TAC	HMS	TAC	HMS
Cora	GCNv2	66.66→64.88	0.991→0.968	72.91→72.26	1.000→0.993	73.14→72.69	1.000→0.992
DBLP	SSG	69.35→68.80	0.986→0.891	71.93→71.46	1.000→0.992	71.94→71.54	1.000→0.989
Photo	SAGE	83.52→78.51	0.974→0.909	86.45→82.86	1.000→0.990	86.62→82.97	1.000→0.992
Computers	ARMA	80.03→76.06	0.876→0.825	82.40→80.91	1.000→1.000	82.49→80.46	1.000→1.000
CS	GEN	89.58→89.72	1.000→1.000	90.65→90.91	1.000→1.000	90.67→90.94	1.000→1.000
Physics	GTF	91.65→91.57	0.990→0.977	92.82→92.86	0.999→0.987	92.80→92.82	1.000→0.992

TABLE IX: Test accuracy (TAC), ownership verification accuracy (OVA), and false positive rate (FPR) of watermarked (or fingerprinted) models and their corresponding surrogate models using the SAGE architecture. Metrics before and after \rightarrow denote the values correspond to the watermarked (or fingerprinted) models and their surrogate models, respectively. Since only *Setting I* is resilient to model extraction attacks, we report results for *Setting I* only.

Datasets	Models	WGB			RBOVG			WGLE <i>Setting I</i>			
		TAC	OVA	FPR	TAC	OVA	FPR	TAC	OVA	FPR	HMS
Cora	GCNv2	70.33→74.82	0.500	0.000	70.33→69.84	1.000	0.000	66.66→71.71	1.000	0.000	0.991→0.872
DBLP	SSG	65.03→71.44	0.500	0.000	65.03→63.04	1.000	0.000	69.35→69.28	1.000	0.000	0.986→0.898
Photo	SAGE	89.69→87.84	0.500	0.000	89.69→89.63	1.000	0.000	83.52→85.66	1.000	0.000	0.974→0.888
Computers	ARMA	85.39→82.18	0.500	0.000	85.39→83.47	1.000	0.000	79.03→81.72	0.510	0.000	0.876→0.682
CS	GEN	90.79→78.07	0.500	0.000	90.79→86.17	1.000	0.000	89.58→75.98	1.000	0.000	1.000→0.895
Physics	GTF	94.58→92.14	0.500	0.000	94.58→94.22	1.000	0.000	91.65→92.08	1.000	0.000	0.990→0.922

versary then trains a surrogate model on these samples. The surrogate model is implemented using the SAGE or SSG architecture and is trained using the Adam optimizer with a learning rate of $1e-4$ for 1500 epochs, with the KL divergence serving as the objective function. We report the TAC, OVA, FPR, and HMS of the surrogate models.

Result Analysis. Table VIII reports the changes in TAC and HMS before and after watermark overwriting. It can be observed that watermark overwriting leads to a decrease in the TAC for all models. In addition, the original watermark remains intact with HMS values above 0.825 for *Setting I*, and above 0.987 for *Setting II* and *III*. The results indicate that overwriting using *Setting III* of WGLE does not compromise the original watermark. It should be noted that the watermarked model now contains two distinct watermarks, a situation commonly encountered in ownership verification. This issue can be addressed by registering the encrypted watermark with a third party (e.g. an intellectual property authority or a blockchain system) along with a timestamp [13]. In such cases, the watermark with the later timestamp will not be recognized as a proof of ownership.

Table IX presents the results of the ownership verification for the surrogate model obtained via model extraction attacks. Since only *Setting I* is robust to such attacks, we report results exclusively for this setting. WGLE achieves 100% OVA and 0 FPR on all models except ARMA on *Computers*, indicating that the watermark remains detectable in most surrogate models. These results confirm that the watermark embedded in the watermarked model can be inherited by the surrogate models. Although WGLE is slightly less than RBOVG against model extraction attacks, it remains effective in most scenarios. WGB fails against model extraction attacks.

The surrogate model retains test accuracy comparable to that of the watermarked model on the primary task without the watermark. The results using SSG as the surrogate model architecture are provided in Appendix F.

Answers to RQ3: Even if the adversary is aware of our watermarking algorithm, they cannot overwrite the original watermark by *Setting III* of WGLE. WGLE is robust against model extraction attacks in most cases.

VII. RELATED WORK

Ownership verification. Copyright protection for machine learning models has attracted significant attention, leading to the development of various watermarking methods. Uchida et al. [30] initiated the first work by embedding bit sequences in the model weights. However, their white-box scheme requires full access to model parameters during ownership verification, limiting its practicality. Adi et al. [33] introduced the first black-box watermarking approach. They embed backdoors into the model to make it output predefined misclassifications for specific samples. This design is the basis for most subsequent methods. However, the use of backdoors introduces serious security risks. EaaW [41] represents the state-of-the-art black-box watermarking, which uses the feature importance explanation as the watermark. However, EaaW is not directly applicable to GNNs.

For GNNs, WGRG [11] is the first GNN black-box watermarking method. WGB [12] extended it to support node-level and graph-level tasks. Other methods such as GENIE [57] and PreGIP [58] focus on link prediction and task-agnostic scenarios, respectively. Despite their contributions, these methods still rely on backdoors, making watermarked GNN models susceptible to backdoor attacks. These limitations motivate the

design of a backdoor-free, multi-bit black-box watermarking paradigm tailored for GNNs.

IP attacks to ownership verification. Existing attacks against ownership verification can be broadly categorized into three types: IP detection, IP removal (also known as ownership obfuscation), and IP ambiguity.

IP detection aims to disrupt ownership verification at the query stage. Since queries involving trigger samples often exhibit distinct characters from normal inference behavior, adversaries can detect and block such queries and refuse to respond [6], [59], [60]. This issue is particularly severe when multiple watermarked models have been distributed, as the verifier must submit all trigger samples corresponding to each watermarked model. In contrast, WGLE eliminates this limitation by requiring only a single query using the same trigger graph, regardless of how many watermarked models have been distributed.

IP removal refers to techniques that remove watermarks or fingerprints from the model by post-processing, including fine-tuning, pruning, or overwriting [6], [61], [62], [63], [64], [65], [66]. Alternatively, the adversary can train a local surrogate model by querying the API of the watermarked model, obtaining a model with a functional approximation without inheriting watermarks or fingerprints [67], [68], [28]. We have demonstrated the robustness of WGLE in Section VI.

IP ambiguity involves forging watermarks or fingerprints to falsely claim ownership. For example, an adversary may collect naturally misclassified samples and present them as triggers to pass ownership verification [23]. However, existing ambiguity attacks target a zero-bit watermark. In contrast, it is significantly more difficult to forge a multi-bit watermark to pass ownership verification. We provide a detailed discussion in the Appendix D.

VIII. FUTURE WORK AND LIMITATION

A. Potential application of LDDE

We outline several potential directions for future work based on LDDE. As each trained GNN model yields unique LDDE values for a given input graph, a promising direction is to explore whether LDDE can act as fingerprints. Since LDDE-based watermarking modifies the distance between connected nodes, and such distances are known to be exploitable in link stealing attacks [38], [39], it is worth investigating whether LDDE modifications undermine the success of these attacks. The distance between the connected nodes is auxiliary information, and we define LDDE to embed the watermark. An extension is to explore whether such distances can encode input-dependent information. For example, an adversary trains and releases a GNN model that produces both accurate predictions and specific output distances for input samples that exhibit specific relationships. The adversary exploits the model output to infer sensitive information about the input data without direct access to it. We leave the exploration of these possibilities to future work.

B. Limitation of WGLE

WGLE achieves a backdoor-free, multi-bit watermarking scheme in the black-box setting for node-level GNNs. However, its applicability is inherently limited to GNNs, as LDDE is a property unique to graph-structured data. Consequently, WGLE is not applicable to conventional neural networks that operate on Euclidean data. Furthermore, WGLE does not support graph-level GNNs in black-box settings. These models employ graph pooling operations to aggregate node embeddings into a single graph-level representation. Without observable edge structures in the outputs, WGLE cannot be achieved in black-box settings. In addition, the applicability of *Setting I* of WGLE is restricted in small-scale training graphs, such as `CorA`. It leads to an unacceptable drop in the model’s performance on the primary task. Although *Setting II* and *Setting III* alleviate this issue, they in turn sacrifice robustness against model extraction attacks. Finally, the experiments (Section VI) reveal dataset-specific weaknesses in robustness. For example, WGLE is less robust against pruning for GEN on `CS`, and less robust against fine-tuning for SSG on `DBLP`. We speculate that robustness is correlated with the number of prediction classes: datasets with many classes (e.g., `CS`) are more sensitive to pruning, whereas those with very few classes (e.g., `DBLP`) are more vulnerable to fine-tuning. This limitation may be mitigated by designing adaptive LDDE distance metrics, which we leave for future work.

C. Additional Benefits of WGLE

WGLE requires only fine-tuning of a trained model to embed the watermark, eliminating the need to retrain the watermarked model from scratch. This significantly reduces the overhead of watermark embedding. As shown in Appendix B, the time cost of WGLE is only 50% of that of WGB and merely 5% of RBOVG. Although ownership collision is an inherent concern, WGLE provides a more transparent and controllable framework. Unlike most prior methods where collision probability is difficult to estimate, the probability in WGLE is determined by the generation of the watermark string, which is quantifiable. We further analyze how this probability relates to the similarity threshold and the length of the watermark string in Appendix D.

IX. CONCLUSIONS

This paper presents WGLE, a novel backdoor-free, multi-bit black-box watermarking paradigm for node-level GNNs. By modifying the LDDE values of selected edges, WGLE embeds watermarks without introducing a backdoor. Its multi-bit capacity enables single-query ownership verification even multiple distributions, which is economical and hardly detected. We further consider practical deployment scenarios, including the small training graph and ownership transfer. Extensive experiments demonstrate that WGLE achieves effectiveness, fidelity, robustness, and lower overhead.

REFERENCES

- [1] M. Harl, S. Weinzierl, M. Stierle, and M. Matzner, "Explainable predictive business process monitoring using gated graph neural networks," *Journal of Decision Systems*, vol. 29, no. suppl, pp. 312–327, 2020.
- [2] L. Lv, J. Cheng, N. Peng, M. Fan, D. Zhao, and J. Zhang, "Auto-encoder based graph convolutional networks for online financial anti-fraud," in *2019 IEEE Conference on Computational Intelligence for Financial Engineering & Economics (CIFER)*. IEEE, 2019, pp. 1–6.
- [3] X. Li, Y. Zhou, N. Dvornik, M. Zhang, S. Gao, J. Zhuang, D. Scheinost, L. H. Staib, P. Ventola, and J. S. Duncan, "Braingnn: Interpretable brain graph neural network for fmri analysis," *Medical Image Analysis*, vol. 74, p. 102233, 2021.
- [4] Q. Tan, N. Liu, and X. Hu, "Deep representation learning for social network analysis," *Frontiers in big Data*, vol. 2, p. 2, 2019.
- [5] W. Fan, Y. Ma, Q. Li, Y. He, E. Zhao, J. Tang, and D. Yin, "Graph neural networks for social recommendation," in *The world wide web conference*, 2019, pp. 417–426.
- [6] N. Lukas, E. Jiang, X. Li, and F. Kerschbaum, "Sok: How robust is image classification deep neural network watermarking?" in *2022 IEEE Symposium on Security and Privacy (SP)*. IEEE, 2022, pp. 787–804.
- [7] Y. Sun, T. Liu, P. Hu, Q. Liao, S. Fu, N. Yu, D. Guo, Y. Liu, and L. Liu, "Deep intellectual property protection: A survey," *arXiv preprint arXiv:2304.14613*, 2023.
- [8] Y. Quan, H. Teng, Y. Chen, and H. Ji, "Watermarking deep neural networks in image processing," *IEEE transactions on neural networks and learning systems*, vol. 32, no. 5, pp. 1852–1865, 2020.
- [9] S. Abdelnabi and M. Fritz, "Adversarial watermarking transformer: Towards tracing text provenance with data hiding," in *2021 IEEE Symposium on Security and Privacy (SP)*. IEEE, 2021, pp. 121–140.
- [10] P. Rath, S. Bhadauria, and S. Rath, "Watermarking of deep recurrent neural network using adversarial examples to protect intellectual property," *Applied Artificial Intelligence*, vol. 36, no. 1, p. 2008613, 2022.
- [11] X. Zhao, H. Wu, and X. Zhang, "Watermarking graph neural networks by random graphs," in *2021 9th International Symposium on Digital Forensics and Security (ISDFS)*. IEEE, 2021, pp. 1–6.
- [12] J. Xu, S. Koffas, O. Ersoy, and S. Picek, "Watermarking graph neural networks based on backdoor attacks," in *2023 IEEE 8th European Symposium on Security and Privacy (EuroS&P)*. IEEE, 2023, pp. 1179–1197.
- [13] A. Waheed, V. Duddu, and N. Asokan, "Grove: Ownership verification of graph neural networks using embeddings," in *2024 IEEE Symposium on Security and Privacy (SP)*. IEEE, 2024, pp. 2460–2477.
- [14] R. Zhou, K. Yang, X. Wang, W. H. Wang, and J. Xu, "Revisiting black-box ownership verification for graph neural networks," in *2024 IEEE Symposium on Security and Privacy (SP)*. IEEE Computer Society, 2024, pp. 210–210.
- [15] L. Du, X. Zhou, M. Chen, C. Zhang, Z. Su, P. Cheng, J. Chen, and Z. Zhang, "Sok: Dataset copyright auditing in machine learning systems," *arXiv preprint arXiv:2410.16618*, 2024.
- [16] X. You, Y. Jiang, J. Xu, M. Zhang, and M. Yang, "Gnnfingers: A fingerprinting framework for verifying ownerships of graph neural networks," in *Proceedings of the ACM on Web Conference 2024*, 2024, pp. 652–663.
- [17] S. Leroux, S. Vanasse, and P. Simoens, "Multi-bit black-box watermarking of deep neural networks in embedded applications," in *Proceedings of the IEEE/CVF Conference on Computer Vision and Pattern Recognition*, 2024, pp. 2121–2130.
- [18] S. Peng, Y. Chen, J. Xu, Z. Chen, C. Wang, and X. Jia, "Intellectual property protection of dnn models," *World Wide Web*, vol. 26, no. 4, pp. 1877–1911, Nov. 2022.
- [19] C. Gong, Z. Yang, Y. Bai, J. He, J. Shi, K. Li, A. Sinha, B. Xu, X. Hou, D. Lo *et al.*, "Baffle: Hiding backdoors in offline reinforcement learning datasets," in *2024 IEEE Symposium on Security and Privacy (SP)*. IEEE, 2024, pp. 2086–2104.
- [20] Y. Li, Y. Jiang, Z. Li, and S.-T. Xia, "Backdoor learning: A survey," *IEEE transactions on neural networks and learning systems*, vol. 35, no. 1, pp. 5–22, 2022.
- [21] Z. Xi, R. Pang, S. Ji, and T. Wang, "Graph backdoor," in *30th USENIX Security Symposium (USENIX Security 21)*, 2021, pp. 1523–1540.
- [22] B. Sun, J. Sun, W. Koh, and J. Shi, "Neural network semantic backdoor detection and mitigation: A {Causality-Based} approach," in *33rd USENIX Security Symposium (USENIX Security 24)*, 2024, pp. 2883–2900.
- [23] J. Liu, R. Zhang, S. Szyller, K. Ren, and N. Asokan, "False claims against model ownership resolution," in *33rd USENIX Security Symposium (USENIX Security 24)*, 2024, pp. 6885–6902.
- [24] S. Han, J. Pool, J. Tran, and W. Dally, "Learning both weights and connections for efficient neural network," *Advances in neural information processing systems*, vol. 28, 2015.
- [25] K. W. Church, Z. Chen, and Y. Ma, "Emerging trends: A gentle introduction to fine-tuning," *Natural Language Engineering*, vol. 27, no. 6, pp. 763–778, 2021.
- [26] D. DeFazio and A. Ramesh, "Adversarial model extraction on graph neural networks," *arXiv preprint arXiv:1912.07721*, 2019.
- [27] B. Wu, X. Yang, S. Pan, and X. Yuan, "Model extraction attacks on graph neural networks: Taxonomy and realisation," in *Proceedings of the 2022 ACM on Asia conference on computer and communications security*, 2022, pp. 337–350.
- [28] Y. Shen, X. He, Y. Han, and Y. Zhang, "Model stealing attacks against inductive graph neural networks," in *2022 IEEE Symposium on Security and Privacy (SP)*. IEEE, 2022, pp. 1175–1192.
- [29] Z. Wu, S. Pan, F. Chen, G. Long, C. Zhang, and S. Y. Philip, "A comprehensive survey on graph neural networks," *IEEE transactions on neural networks and learning systems*, vol. 32, no. 1, pp. 4–24, 2020.
- [30] Y. Uchida, Y. Nagai, S. Sakazawa, and S. Satoh, "Embedding watermarks into deep neural networks," in *Proceedings of the 2017 ACM on International Conference on Multimedia Retrieval*, ser. ICMR '17. ACM, Jun. 2017.
- [31] Z. Li, C. Hu, Y. Zhang, and S. Guo, "How to prove your model belongs to you: A blind-watermark based framework to protect intellectual property of dnn," in *Proceedings of the 35th Annual Computer Security Applications Conference*, 2019, pp. 126–137.
- [32] Y. Lao, P. Yang, W. Zhao, and P. Li, "Identification for deep neural network: Simply adjusting few weights!" in *2022 IEEE 38th International Conference on Data Engineering (ICDE)*. IEEE, 2022, pp. 1328–1341.
- [33] Y. Adi, C. Baum, M. Cisse, B. Pinkas, and J. Keshet, "Turning your weakness into a strength: Watermarking deep neural networks by backdooring," in *27th USENIX Security Symposium (USENIX Security 18)*, 2018, pp. 1615–1631.
- [34] Y. Li, Y. Bai, Y. Jiang, Y. Yang, S.-T. Xia, and B. Li, "Untargeted backdoor watermark: Towards harmless and stealthy dataset copyright protection," *Advances in Neural Information Processing Systems*, vol. 35, pp. 13 238–13 250, 2022.
- [35] E. Dai, T. Zhao, H. Zhu, J. Xu, Z. Guo, H. Liu, J. Tang, and S. Wang, "A comprehensive survey on trustworthy graph neural networks: Privacy, robustness, fairness, and explainability," *Machine Intelligence Research*, pp. 1–51, 2024.
- [36] H. Jia, C. A. Choquette-Choo, V. Chandrasekaran, and N. Papernot, "Entangled watermarks as a defense against model extraction," in *30th USENIX security symposium (USENIX Security 21)*, 2021, pp. 1937–1954.
- [37] Y. Li, Y. Bai, Y. Jiang, Y. Yang, S.-T. Xia, and B. Li, "Untargeted backdoor watermark: Towards harmless and stealthy dataset copyright protection," *Advances in Neural Information Processing Systems*, vol. 35, pp. 13 238–13 250, 2022.
- [38] X. He, J. Jia, M. Backes, N. Z. Gong, and Y. Zhang, "Stealing links from graph neural networks," in *30th USENIX security symposium (USENIX security 21)*, 2021, pp. 2669–2686.
- [39] F. Wu, Y. Long, C. Zhang, and B. Li, "Linkteller: Recovering private edges from graph neural networks via influence analysis," in *2022 IEEE Symposium on Security and Privacy (SP)*. IEEE, 2022, pp. 2005–2024.
- [40] D. Steinley, "Properties of the hubert-arable adjusted rand index," *Psychological methods*, vol. 9, no. 3, p. 386, 2004.
- [41] S. Shao, Y. Li, H. Yao, Y. He, Z. Qin, and K. Ren, "Explanation as a watermark: Towards harmless and multi-bit model ownership verification via watermarking feature attribution," *arXiv preprint arXiv:2405.04825*, 2024.
- [42] X. Luo, Y. Wu, X. Xiao, and B. C. Ooi, "Feature inference attack on model predictions in vertical federated learning," in *2021 IEEE 37th international conference on data engineering (ICDE)*. IEEE, 2021, pp. 181–192.
- [43] Z. Yang, W. Cohen, and R. Salakhudinov, "Revisiting semi-supervised learning with graph embeddings," in *International conference on machine learning*. PMLR, 2016, pp. 40–48.
- [44] A. Grover and J. Leskovec, "node2vec: Scalable feature learning for networks," in *Proceedings of the 22nd ACM SIGKDD international*

- conference on Knowledge discovery and data mining, 2016, pp. 855–864.
- [45] E. Schubert, J. Sander, M. Ester, H. P. Kriegel, and X. Xu, “Dbscan revisited, revisited: why and how you should (still) use dbscan,” *ACM Transactions on Database Systems (TODS)*, vol. 42, no. 3, pp. 1–21, 2017.
- [46] X. Deng and Z. Zhang, “Graph-free knowledge distillation for graph neural networks,” *arXiv preprint arXiv:2105.07519*, 2021.
- [47] Y. Zhuang, L. Lyu, C. Shi, C. Yang, and L. Sun, “Data-free adversarial knowledge distillation for graph neural networks,” *arXiv preprint arXiv:2205.03811*, 2022.
- [48] N. Dehmamy, A.-L. Barabási, and R. Yu, “Understanding the representation power of graph neural networks in learning graph topology,” *Advances in Neural Information Processing Systems*, vol. 32, 2019.
- [49] A. Bojchevski and S. Günnemann, “Deep gaussian embedding of graphs: Unsupervised inductive learning via ranking,” *arXiv preprint arXiv:1707.03815*, 2017.
- [50] O. Shchur, M. Mumme, A. Bojchevski, and S. Günnemann, “Pitfalls of graph neural network evaluation,” *arXiv preprint arXiv:1811.05868*, 2018.
- [51] M. Chen, Z. Wei, Z. Huang, B. Ding, and Y. Li, “Simple and deep graph convolutional networks,” in *International conference on machine learning*. PMLR, 2020, pp. 1725–1735.
- [52] Y. Shi, Z. Huang, S. Feng, H. Zhong, W. Wang, and Y. Sun, “Masked label prediction: Unified message passing model for semi-supervised classification,” *arXiv preprint arXiv:2009.03509*, 2020.
- [53] W. Hamilton, Z. Ying, and J. Leskovec, “Inductive representation learning on large graphs,” *Advances in neural information processing systems*, vol. 30, 2017.
- [54] H. Zhu and P. Koniusz, “Simple spectral graph convolution,” in *International conference on learning representations*, 2021.
- [55] G. Li, C. Xiong, A. Thabet, and B. Ghanem, “Deepergcn: All you need to train deeper gcns,” *arXiv preprint arXiv:2006.07739*, 2020.
- [56] F. M. Bianchi, D. Grattarola, L. Livi, and C. Alippi, “Graph neural networks with convolutional arma filters,” *IEEE transactions on pattern analysis and machine intelligence*, vol. 44, no. 7, pp. 3496–3507, 2021.
- [57] V. S. P. Bachina, A. Gangwal, A. A. Sharma, and C. Sharma, “Genie: Watermarking graph neural networks for link prediction,” *arXiv preprint arXiv:2406.04805*, 2024.
- [58] E. Dai, M. Lin, and S. Wang, “Pregip: Watermarking the pretraining of graph neural networks for deep intellectual property protection,” *arXiv preprint arXiv:2402.04435*, 2024.
- [59] R. Namba and J. Sakuma, “Robust watermarking of neural network with exponential weighting,” in *Proceedings of the 2019 ACM Asia Conference on Computer and Communications Security*, 2019, pp. 228–240.
- [60] W. Xu, D. Evans, and Y. Qi, “Feature squeezing: Detecting adversarial examples in deep neural networks,” *arXiv preprint arXiv:1704.01155*, 2017.
- [61] X. Chen, W. Wang, Y. Ding, C. Bender, R. Jia, B. Li, and D. Song, “Leveraging unlabeled data for watermark removal of deep neural networks,” in *ICML workshop on Security and Privacy of Machine Learning*, 2019, pp. 1–6.
- [62] X. Liu, F. Li, B. Wen, and Q. Li, “Removing backdoor-based watermarks in neural networks with limited data,” in *2020 25th International Conference on Pattern Recognition (ICPR)*. IEEE, 2021, pp. 10 149–10 156.
- [63] Z. Zhong, L. Zheng, G. Kang, S. Li, and Y. Yang, “Random erasing data augmentation,” in *Proceedings of the AAAI conference on artificial intelligence*, vol. 34, no. 07, 2020, pp. 13 001–13 008.
- [64] T. D. Nguyen, P. Rieger, R. De Viti, H. Chen, B. B. Brandenburg, H. Yalame, H. Möllering, H. Fereidooni, S. Marchal, M. Miettinen *et al.*, “[FLAME]: Taming backdoors in federated learning,” in *31st USENIX Security Symposium (USENIX Security 22)*, 2022, pp. 1415–1432.
- [65] B. Wang, Y. Yao, S. Shan, H. Li, B. Viswanath, H. Zheng, and B. Y. Zhao, “Neural cleanse: Identifying and mitigating backdoor attacks in neural networks,” in *2019 IEEE symposium on security and privacy (SP)*. IEEE, 2019, pp. 707–723.
- [66] Y. Yan, X. Pan, M. Zhang, and M. Yang, “Rethinking {White-Box} watermarks on deep learning models under neural structural obfuscation,” in *32nd USENIX Security Symposium (USENIX Security 23)*, 2023, pp. 2347–2364.
- [67] S. Lee, W. Song, S. Jana, M. Cha, and S. Son, “Evaluating the robustness of trigger set-based watermarks embedded in deep neural networks,”

IEEE Transactions on Dependable and Secure Computing, vol. 20, no. 4, pp. 3434–3448, 2022.

- [68] Y. Zhuang, C. Shi, M. Zhang, J. Chen, L. Lyu, P. Zhou, and L. Sun, “Unveiling the secrets without data: Can graph neural networks be exploited through {Data-Free} model extraction attacks?” in *33rd USENIX Security Symposium (USENIX Security 24)*, 2024, pp. 5251–5268.

APPENDIX A

TRANSFORMATION OF THE SOFTMAX FUNCTION

Softmax is a common function used in multi-class classification to convert a vector of real numbers $\mathbf{z} = [z_1, z_2, \dots, z_n]$ into a probability distribution. It is defined as:

$$\mathcal{S}(\mathbf{z}) = \left[\frac{e^{z_1}}{\sum_{i=1}^n e^{z_i}}, \frac{e^{z_2}}{\sum_{i=1}^n e^{z_i}}, \dots, \frac{e^{z_n}}{\sum_{i=1}^n e^{z_i}} \right]$$

where n is the number of classes, and $\mathcal{S}(\cdot)$ represents the softmax operation. The softmax ensures that all probabilities sum to 1, making them suitable for classification tasks. It is typically used in conjunction with cross-entropy loss.

To normalize the posterior probabilities derived from softmax, we apply a log transformation followed by mean and standard deviation normalization [42]:

$$\begin{aligned} \log(\mathcal{S}(\mathbf{z})) &= [z_1 - C, z_2 - C, \dots, z_n - C], C = \log\left(\sum_{i=1}^n e^{z_i}\right) \\ \mu(\log(\mathcal{S}(\mathbf{z}))) &= \frac{1}{n} \sum_{i=1}^n (z_i - C) = \mu(\mathbf{z}) - C \\ \sigma(\log(\mathcal{S}(\mathbf{z}))) &= \sqrt{\frac{1}{n-1} \sum_{i=1}^n (z_i - C - (\mu(\mathbf{z}) - C))^2} = \sigma(\mathbf{z}) \\ \frac{\log(\mathcal{S}(\mathbf{z})) - \mu(\log(\mathcal{S}(\mathbf{z})))}{\sigma(\log(\mathcal{S}(\mathbf{z})))} &= \frac{\mathbf{z} - \mu(\mathbf{z})}{\sigma(\mathbf{z})} \end{aligned}$$

The normalized log-transformed posterior probabilities $\mathcal{S}(\mathbf{z})$ are equivalent to directly normalizing the embeddings \mathbf{z} .

APPENDIX B

OVERHEAD

Table X presents the average generation time of the watermarked or fingerprinted models. WGLE stops fine-tuning once the watermark is successfully embedded. WGB uses a fixed 500-epoch to train the watermarked model. RBOVG follows the default setting, training 60 independently trained models and 60 surrogate models to build the ownership classifier. WGLE consistently incurs a lower computational overhead compared to both WGB and RBOVG. For smaller graphs (CoRa), *Setting I* achieves the lowest overhead, whereas *Setting II* is more efficient for larger graphs (Physics). In general, the computational cost of WGLE is approximately 50% of that of WGB and only 5% of that of RBOVG.

APPENDIX C

HARM OF BACKDOOR

Table XI demonstrates the potential harm introduced by backdoor-based watermarking. In WGB, class “2” is designated as the target label. As shown, once the backdoor pattern is embedded in the input features, more than 83% of these

TABLE X: Time overhead of embedding watermarks or constructing fingerprints. The unit is seconds.

Datasets	Models	WGB	RBOVG	Setting I	Setting II	Setting III
Cora	GCNv2	3.07	16.24	1.64	2.75	2.81
DBLP	SSG	5.81	52.45	2.66	3.29	3.23
Photo	SAGE	3.39	126.26	2.22	2.22	2.23
Computers	ARMA	7.42	245.20	4.21	3.02	3.03
CS	GEN	13.81	598.99	6.01	7.45	7.49
Physics	GTF	50.52	1241.70	21.13	17.95	17.93

TABLE XI: We designate label “2” as the target class and evaluate the rate at which non-“2” samples are misclassified as class “2” once using backdoors. \mathcal{M}_o is the original model.

Datasets	Models	\mathcal{M}_o	WGB	Setting I	Setting II	Setting III
Cora	GCNv2	0.021	0.950	0.036	0.036	0.040
DBLP	SSG	0.036	1.000	0.045	0.041	0.040
Photo	SAGE	0.002	0.975	0.002	0.002	0.002
Computers	ARMA	0.006	0.895	0.007	0.005	0.006
CS	GEN	0.009	1.000	0.017	0.016	0.015
Physics	GTF	0.035	0.830	0.042	0.038	0.039

samples are misclassified as class “2” by the watermarked model. In contrast, the original model and WGLE under *Settings I, II, and III* maintain misclassification rates below 4.5%. These vulnerabilities pose significant risks in security-critical scenarios. For example, if a GNN model is deployed for malicious user detection, an adversary could exploit the backdoor to craft input that misleads the model into classifying a malicious user as benign.

APPENDIX D WATERMARK COLLISION

Given two independently generated watermark strings, where each bit is sampled from a Bernoulli(0.5) distribution, their expected bitwise match rate (i.e., Hamming similarity) is 0.5. When the watermark length is sufficiently large, the HMS approximately follows a normal distribution with mean 0.5 due to the Central Limit Theorem.

To empirically validate this conclusion, we conducted experiments using SAGE on *Photo* and GTF on *Physics*. Specifically, we generated 100 watermarked models, each embedded with a distinct 200-bit randomly generated watermark string. We then measured the HMS between the target watermark and the extracted watermark from another watermarked model without the target watermark.

As shown in Figure 6, the HMS values observed in *Setting I, II, and III* closely follow a normal distribution centered around 0.5 with a standard deviation of approximately 0.35, consistent with our theoretical expectation.

We formally define the concept of watermark collision and derive the relationship between the collision probability α and the similarity threshold τ as follows:

$$\mathbb{P}(\text{HMS} \geq \tau) \leq \alpha. \quad (8)$$

where HMS denotes the Hamming similarity between two randomly generated watermark strings.

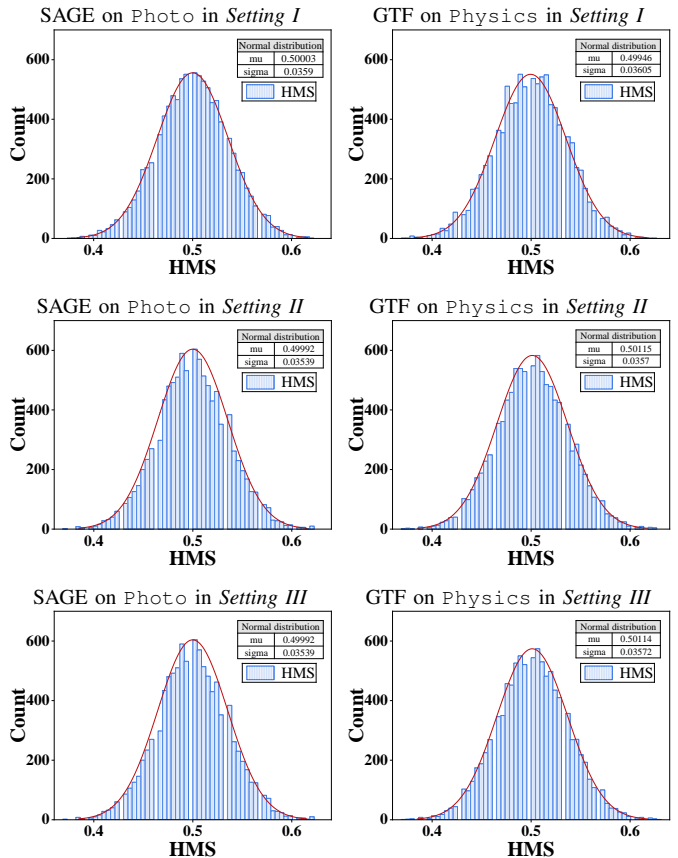


Fig. 6: HMS between the target watermark and the extracted watermark from another watermarked model without the target watermark.

When the watermark length N_w is sufficiently large, HMS can be approximated by a normal distribution:

$$\text{HMS} \sim \mathcal{N}\left(0.5, \frac{1}{4N_w}\right). \quad (9)$$

which is normalized as:

$$\frac{\text{HMS} - 0.5}{\sqrt{1/(4N_w)}} \sim \mathcal{N}(0, 1), \quad (10)$$

we derive the collision probability:

$$\tau \geq 0.5 + \Phi^{-1}(1 - \alpha) \cdot \sqrt{\frac{1}{4N_w}} \quad (11)$$

where $\Phi^{-1}(1 - \alpha)$ denotes the inverse CDF of the standard normal distribution at confidence level $1 - \alpha$

Equation 11 captures the relationship among the watermark length N_w , the similarity threshold τ , and the collision probability α . For example, with $N_w = 200$ and $\tau = 0.75$ as used in our experiments, the resulting collision probability is $\alpha \approx 7.69 \times 10^{-13}$. In practice, these parameters can be selected based on the requirements of the application. If the watermark strings are not fully independent (e.g., containing fixed segments or timestamps generated within a short time

TABLE XII: Impact of the length of the watermark string on fidelity and robustness. “Test” denotes the cross-entropy loss (CE) of the watermarked model on the test graph for the primary task. “Pruning” and “Fine-tuning” represent the binary cross-entropy (BCE) between the target watermark string and the extracted watermark string from the watermarked model after pruning or fine-tuning. Cora contains fewer than 500 eligible edges.

Dataset	Model	N_w	Setting I			Setting II			Setting III		
			Test	Pruning	Fine-tuning	Test	Pruning	Fine-tuning	Test	Pruning	Fine-tuning
Cora	GCNv2	20	1.8024	0.3336	0.4316	1.4133	0.3149	0.3368	1.3494	0.3228	0.3288
		100	2.7539	0.3567	0.4477	1.5412	0.3210	0.3469	1.5322	0.3245	0.3485
		200	4.1743	0.3605	0.5101	1.6125	0.3273	0.3562	1.7666	0.3297	0.3614
DBLP	SSG	20	1.6330	0.3595	0.3595	1.5629	0.3633	0.4120	1.5949	0.4111	0.4257
		100	2.6147	0.5004	0.5004	1.6355	0.4468	0.4902	1.5935	0.4048	0.4345
		200	1.9021	0.4239	0.4239	1.7129	0.4361	0.4909	1.6869	0.4426	0.4878
Photo	SAGE	20	0.5052	0.5001	0.5727	0.4965	0.3251	0.3367	0.5277	0.3235	0.3354
		100	0.5628	0.4410	0.4686	0.4699	0.3305	0.3491	0.4908	0.3273	0.3357
		200	0.6292	0.4808	0.5118	0.5028	0.3359	0.3612	0.5336	0.3485	0.3844
Computers	ARMA	20	0.6463	0.6023	0.5364	0.5547	0.4425	0.3489	0.5626	0.4346	0.3507
		100	0.7281	0.6160	0.5255	0.5630	0.4802	0.3551	0.5573	0.5096	0.3680
		200	0.7310	0.6243	0.5597	0.5608	0.5009	0.3935	0.5635	0.5176	0.3851
CS	GEN	20	0.8167	0.5314	0.3550	0.8313	0.5598	0.3336	0.8294	0.6495	0.3327
		100	0.8325	0.5818	0.3997	0.8217	0.5460	0.3309	0.8191	0.5086	0.3289
		200	0.8499	0.5689	0.4417	0.8232	0.6496	0.3348	0.8221	0.5947	0.3386
Physics	GTF	20	0.4208	0.3272	0.3756	0.3406	0.3490	0.4117	0.3511	0.3499	0.3840
		100	0.4033	0.3518	0.3996	0.3486	0.3723	0.4302	0.3577	0.3497	0.3848
		200	0.4312	0.3518	0.4460	0.3439	0.3533	0.4444	0.3474	0.3635	0.4428
		500	0.4876	0.3579	0.4804	0.3681	0.4074	0.4821	0.3578	0.3895	0.4947

interval), a higher similarity threshold τ is necessary to ensure a small collision probability α .

APPENDIX E MULTI-BIT

We examine the impact of the length of the watermark string ($N_w = 20, 100, 200, 500$) on the fidelity and robustness of the watermarked model. We compute the cross-entropy (CE) between the model predictions and ground-truth labels on the test graph to evaluate fidelity, where lower CE values indicate better predictive performance. Accuracy is not used, as it fails to capture subtle shifts in confidence. For example, a prediction confidence drop from 95% to 85% does not affect classification accuracy, but increases cross-entropy loss. Similarly, we adopt binary cross-entropy (BCE) as an alternative to Hamming similarity for evaluating watermark matching, where lower BCE values indicate greater similarity to the target watermark string.

As shown in Table XII, the cross-entropy (CE) of the watermarked model on the test graph increases as the length of the watermark string increases, indicating that a longer watermark string has a greater impact on the fidelity. In addition, longer watermark strings also reduce the robustness of the watermarked model. However, this does not imply that shorter watermarks are always preferable, as shorter strings result in a higher probability of watermark collision.

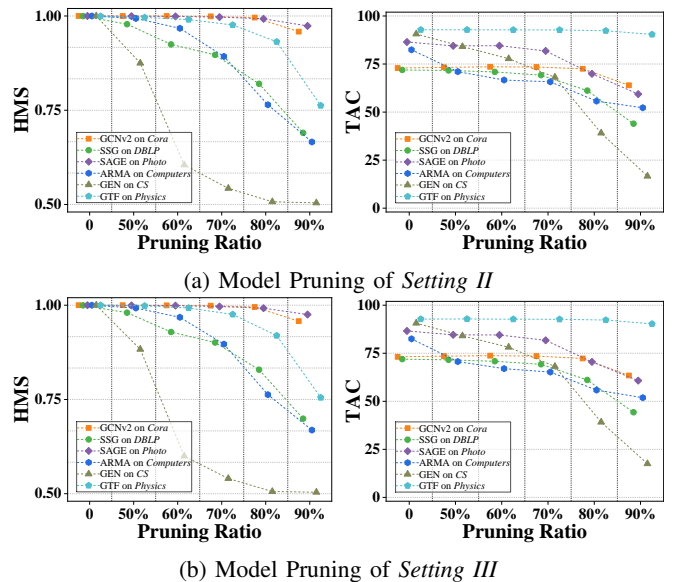


Fig. 7: Hamming similarity (HMS) and test accuracy (TAC) of watermarked models against model pruning in *Setting II* and *Setting III*.

APPENDIX F ADDITIONAL EXPERIMENTAL RESULTS

We provide additional experimental results here that could not be included in the main paper due to space constraints.

TABLE XIII: Test accuracy (TAC), ownership verification accuracy (OVA), and false positive rate (FPR) of watermarked (or fingerprinted) models and their corresponding surrogate models using the SSG architecture. Metrics before and after \rightarrow denote the values correspond to the watermarked (or fingerprinted) models and their surrogate models, respectively. Since only *Setting I* is resilient to model extraction attacks, we report results for *Setting I* only.

Datasets	Models	WGB			RBOVG			WGLE <i>Setting I</i>			
		TAC	OVA	FPR	TAC	OVA	FPR	TAC	OVA	FPR	HMS
Cora	GCNv2	70.33 \rightarrow 71.97	0.500	0.000	70.33 \rightarrow 69.84	1.000	0.000	66.66 \rightarrow 67.75	1.000	0.000	0.991 \rightarrow 0.876
DBLP	SSG	65.03 \rightarrow 71.73	0.500	0.000	65.03 \rightarrow 63.04	1.000	0.000	69.35 \rightarrow 69.58	1.000	0.000	0.986 \rightarrow 0.971
Photo	SAGE	89.69 \rightarrow 88.24	0.500	0.000	89.69 \rightarrow 89.63	1.000	0.000	83.52 \rightarrow 85.70	1.000	0.000	0.974 \rightarrow 0.851
Computers	ARMA	85.39 \rightarrow 83.49	0.500	0.000	85.39 \rightarrow 83.47	1.000	0.000	79.03 \rightarrow 81.06	0.510	0.000	0.876 \rightarrow 0.686
CS	GEN	90.79 \rightarrow 83.74	0.500	0.000	90.79 \rightarrow 86.17	1.000	0.000	89.58 \rightarrow 81.64	1.000	0.000	1.000 \rightarrow 0.894
Physics	GTF	94.58 \rightarrow 92.78	0.500	0.000	94.58 \rightarrow 94.39	1.000	0.000	91.65 \rightarrow 92.61	1.000	0.000	0.990 \rightarrow 0.888

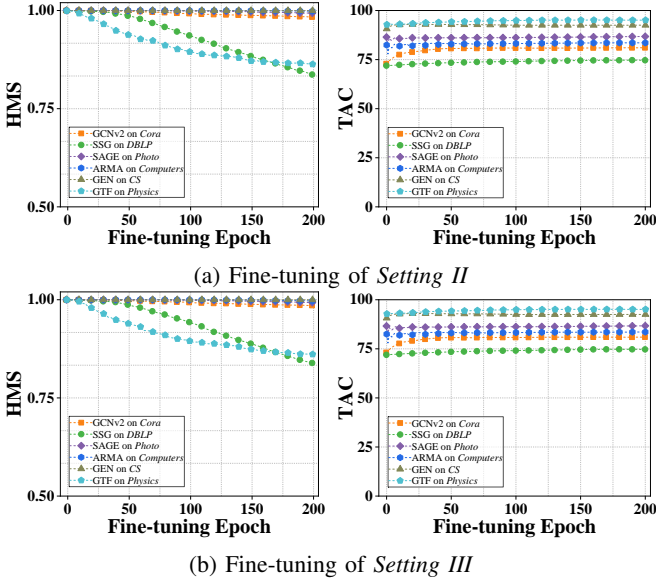


Fig. 8: Hamming similarity (HMS) and test accuracy (TAC) of watermarked models against fine-tuning in *Setting II* and *Setting III*.

Pruning. As shown in Figure 7, *Setting II* and *III* exhibit comparable pruning robustness compared to *Setting I*.

Fine-tuning. *Setting II* and *III* demonstrate stronger robustness against fine-tuning than *Setting I*. As shown in Figure 8, after 200 epochs of fine-tuning, SSG on DBLP exhibits a noticeable decrease in HMS, while GTF on Physics shows a minor decline. All other models maintain an HMS of 1.0. This is likely due to the use of a generated graph as the trigger graph, which leads to a separation between the watermark extraction task and the primary task. Therefore, fine-tuning the watermarked model for the primary task is difficult to impact on the watermark extraction task.

Model extraction attacks. We also present results when the surrogate model using SSG architecture in model extraction attacks. As shown in Table XIII, similar results are observed with the SAGE architecture, ARMA on Computers is the only case where ownership verification fails.

Insight. Additional results of observation-2 and observation-3 for other models and datasets are presented in Figure 9 10.

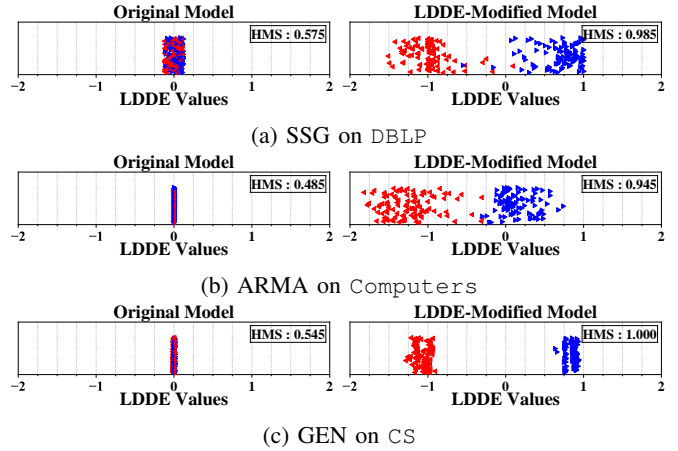


Fig. 9: Projections of LDDE values of selected edges before and after modification. Blue points represent edges targeted for positive LDDE signs, while red points represent edges targeted for negative LDDE signs.

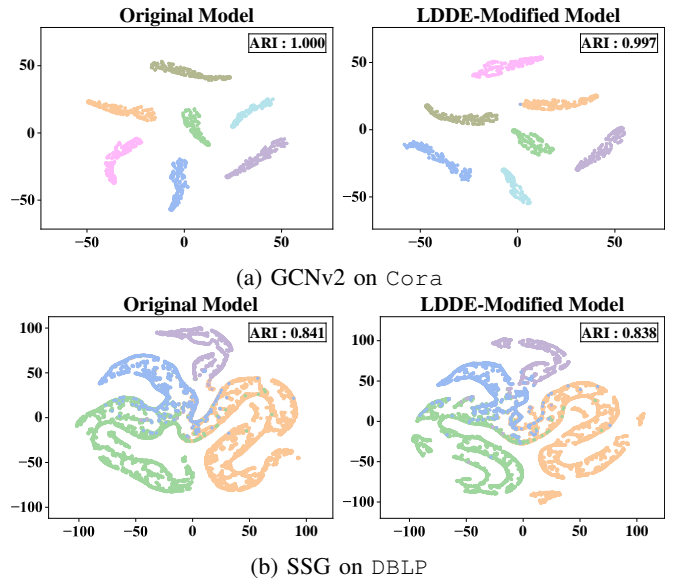


Fig. 10: t-SNE projections of the predictions from both the original and watermarked models. Different colors indicate different classes.